Arabian Journal of Chemistry (2020) **13**, 7115–7131

King Saud University

Arabian Journal of Chemistry

www.ksu.edu.sa
www.sciencedirect.com

ORIGINAL ARTICLE

Efficient synthesis of magnetic nanoparticle-*Musa acuminata* peel composite for the adsorption of anionic dye

Kovo G. Akpomie [a,b,*], **Jeanet Conradie** [a,**]

[a] *Physical Chemistry Research Laboratory, Department of Chemistry, University of the Free State, Bloemfontein, South Africa*
[b] *Department of Pure and Industrial Chemistry, University of Nigeria, Nsukka, Nigeria*

Received 4 May 2020; accepted 27 July 2020
Available online 5 August 2020

KEYWORDS

Bromophenol blue;
Bio-waste;
Nanoparticle;
Magnetite;
Water-treatment

Abstract The impregnation of magnetite (Mt) nanoparticle (NPs) onto *Musa acuminata* peel (MApe), to form a novel magnetic combo (MApe-Mt) for the adsorption of anionic bromophenol blue (BPB) was studied. The SEM, EDX, BET, XRD, FTIR and TGA were used to characterize the adsorbents. The FTIR showed that the OH and C═O groups were the major sites for BPB uptake onto the adsorbent materials. The average Mt crystalline size on MApe-Mt was 21.13 nm. SEM analysis revealed that Mt NPs were agglomerated on the surface of the MApe biosorbent, with an average Mt diameter of 25.97 nm. After Mt impregnation, a decrease in BET surface area (14.89 to 3.80 m^2/g) and an increase in pore diameter (2.25–3.11 nm), pore volume (0.0052–0.01418 cm^3/g) and pH point of zero charge (6.4–7.2) was obtained. The presence of Pb(II) ions in solution significantly decreased the uptake of BPB onto both MApe (66.1–43.8%) and MApe-Mt (80.3–59.1%), compared to other competing ions (Zn(II), Cd(II), Ni(II)) in the solution. Isotherm modeling showed that the Freundlich model best fitted the adsorption data ($R^2 > 0.994$ and SSE < 0.0013). In addition, maximum monolayer uptake was enhanced from 6.04 to 8.12 mg/g after Mt impregnation. Kinetics were well described by the pseudo-first order and liquid film diffusion models. Thermodynamics revealed a physical, endothermic adsorption of BPB onto the adsorbents, with ΔH^o values of 15.87–16.49 kJ/mol, corroborated by high desorption (over 90%) of BPB from the loaded materials. The viability of the prepared adsorbents was also revealed in its reusability for BPB uptake.

* Corresponding author at: Physical Chemistry Research Laboratory, Department of Chemistry, University of the Free State, Bloemfontein, South Africa.
** Corresponding author.
E-mail addresses: kovo.akpomie@unn.edu.ng, 2018711040@ufs4life.ac.za (K.G. Akpomie), conradJ@ufs.ac.za (J. Conradie).
Peer review under responsibility of King Saud University.

Production and hosting by Elsevier

https://doi.org/10.1016/j.arabjc.2020.07.017

1. Introduction

Dyes are useful substances due to their ability to interact with various materials and fabrics to provide beautiful colours. The cosmetic, textile, food, plastic, carpet, printing and leather industries are the major consumers of dyes (An et al., 2019b; Mtshatsheni et al., 2019). Among these industries, the textile industry is the largest consumer of dyes, with a global use of about 700,000 tons of dye annually (Aguayo-Villarreal et al., 2020). As a result, a significant amount of dyes are released from the textile industrial wastewaters into the environment (Ali et al., 2018b). This causes serious water pollution with severe adverse effects to the ecosystem, which is a cause for serious concern (An et al., 2020b; Xia et al., 2020; Zhang et al., 2020). Dyes are difficult to remove from water due to their high stability, which promotes resistance to biological and photo-degradation (El-Gamal et al., 2015). They also reduce the penetration of light into water bodies, affecting the photosynthetic activities of aquatic plants (An et al., 2020a; Chen et al., 2018). In addition, their products of degradation in environmental water can be mutagenic, carcinogenic and cause damage to the skin, brain, liver, and kidneys, as well as to the central nervous and reproductive systems (Madrakian et al., 2013; Mtshatsheni et al., 2019; Oyekanmi et al., 2019; You et al., 2019). Therefore, the treatment of dye containing effluents before their discharge into the environment is vital. Most previous studies have focused on the removal of dyes such as methylene blue and congo red (Dbik et al., 2020; Görgün et al., 2019; Song et al., 2018), with only few reports on bromophenol blue (BPB), a widely used and toxic dye (Dhananasekaran et al., 2016; Mazaheri et al., 2016; Xiang et al., 2019). Hence, the removal of BPB dye from industrial wastewater should also be given significant attention.

Dyes and other pollutants are usually removed from industrial wastewater using processes such as solvent extraction, ion-exchange, precipitation, oxidation, reduction, photocatalytic degradation, filtration, coagulation, flocculation and adsorption (Dawodu and Akpomie, 2016; El-Zahhar et al., 2014; Nassar et al., 2019; Shi et al., 2020a; Singh et al., 2020a; Song et al., 2020). However, most of these methods are capital intensive, complicated, may be inefficient and require skilled personnel. The adsorption process of contaminants onto bio-materials, known as biosorption, is the preferred method, due to its simplicity, low cost, effectiveness, biodegradability and reusability (An et al., 2019a; Crini et al., 2019; Dil et al., 2016; Kocaman, 2020). Therefore, several bio-materials such as micro-organisms, rice husk, orange peels, corncob, groundnut shell, cotton wastes, sugarcane bagasse, just to mention a few, have been successfully applied for the biosorption of dyes and other pollutants (Ali et al., 2018a; De Gisi et al., 2016; Gautam et al., 2014). Among these biosorbents, banana (*Musa acuminata*) peel (MApe) has been reported to be highly efficient for the uptake of various kind of pollutants even in its natural form (Ahmad and Danish, 2018; Akpomie and Conradie, 2020). In addition, the fruit is the world's second largest fruit crop, grown in different parts of the world, thus generating huge amounts of peel bio-waste that can be harnessed easily and cheaply (Akpomie and Conradie, 2020). However, this widely available, low-cost and efficient bio-waste has not yet been utilized for the biosorption of BPB. We thus evaluated the use of MApe for the removal of BPB, while simultaneously recycling bio-waste.

In addition, recent research trends have proven the synthesis and use of nanoparticles (NPs) for the adsorption of dyes and other pollutants to be very effective (Ali et al., 2019a, 2017; Alipanahpour Dil et al., 2018; Mehrabi and Alipanahpour Dil, 2017; Nassar et al., 2018, 2017). These NPs are produced by several techniques such as green-synthesis, sol-gel, hydrothermal, co-precipitation, chemical vapour deposition and chemical reduction (Dai et al., 2020; Fu et al., 2020; Kaur et al., 2019; Luo et al., 2018; Shi et al., 2019, 2020b; Sun et al., 2020; Wang et al., 2020; Zhao et al., 2019). However, the application of NPs for adsorption of contaminants from wastewater is limited by the difficulty in recovering the loaded NP adsorbent from the treated water, due to their small sizes (Ali et al., 2019d). Therefore, the impregnation of these NPs on a suitable substrate (support) to form composite adsorbents have instead become popular to combat this limitation. Researchers found that the loading of metallic NPs on adsorbent surfaces significantly enhances their uptake of dyes and other pollutants (Ali et al., 2019c; Alipanahpour Dil et al., 2019; Du et al., 2020; Li et al., 2019). Among various NPs, the magnetite (Mt) nanoparticle is the most promising and has received significant attention (Abdel-Ghani et al., 2019; Ali et al., 2019b; Ge et al., 2019; Islam et al., 2020; Khoshsang et al., 2018; Mtshatsheni et al., 2019; Muhammad et al., 2019; Nsom et al., 2019). This is ascribed to the efficient catalytic activity of Mt, its good compatibility with adsorbents, as well as the ease of recovery of the loaded adsorbent from the waste solution by magnetic attraction. Furthermore, Mt (Fe_3O_4) is the most magnetic of all the naturally occurring minerals, and is very useful in adsorption studies.

A thorough literature search showed that such nano-magnetic treatment, such as biosorbent surfaces loaded with Mt metallic NPs, has not yet been applied for the adsorption of BPB. In addition, there is presently no report yet on the impregnation of Mt nanoparticles on MApe biosorbent to form a magnetic composite adsorbent. Thus, this study reports for the first time the impregnation of Mt NPs on MApe to form a novel magnetic composite (MApe-Mt), which was applied for the adsorption of BPB dye from solution. The influence of various operating conditions on the BPB uptake was studied, as well as the kinetics, thermodynamics, and isotherms of the biosorption. The regeneration and reusability of the adsorbents were further evaluated to provide a comprehensive report on the efficiency of our prepared adsorbents.

2. Experimental

2.1. Materials and reagents used

The *Musa acuminata* (banana) was obtained from Checkers, Mimosa mall, Bloemfontein, South Africa. Sodium hydroxide (NaOH), hydrochloric acid (HCl), bromophenol blue ($C_{19}H_{10}Br_4O_5S$), nickel (II) acetate tetrahydrate ($Ni(CH_3COO)_2{\cdot}4H_2O$) and cadmium chloride monohydrate ($CdCl_2{\cdot}H_2O$), were purchased from Sigma-Aldrich. The ferric chloride ($FeCl_3$) and ferrous sulphate ($FeSO_4{\cdot}7H_2O$), were obtained from Merck, while lead nitrate ($Pb(NO_3)_2$) and zinc sulphate ($Zn(SO_4)_2$),

were purchased from Fluka. All the chemicals were of analytical grade and used without any purification.

2.2. Preparation of magnetite nanoparticle impregnated Musa acuminata peel

The peels of *Musa acuminata* were removed and washed with tap water to get rid of dirt. It was cut into smaller sizes and sundried for 48 h, then oven dried for 24 h at 80 ^{O}C. Thereafter, the dried samples were pulverized into fine powder using a mortar and pestle and designated as MApe. The composite adsorbent was prepared by thermo-chemical precipitation reaction in solution, by firstly dissolving $FeCl_3$ (2.37 g; 73.06 mM) and $FeSO_4{\cdot}7H_2O$ (2.04 g; 35.97 mM) in 200 mL distilled water on a hot plate and stirred for 1 h at 70 °C. The stirring was done to ensure proper dissolution of the added salts. Then 9.0 g of the prepared MApe was added with constant stirring for 30 min. A colour change from light brown to black-brown was observed. This was followed by the gradual addition of 0.5 M NaOH, until the solution pH was 11.0. The solution was stirred continuously for 2 h and a black solution was observed. The solution was centrifuged at 7000 rpm for 50 min and the residue washed with excess distilled water until neutral pH. The centrifugation was then repeated and the residue was dried in an oven at 80 °C for 2 h. The dried composite was further pulverized to fine powder using a mortar and pestle and sieved through 100 μm mesh to obtain Mt nanoparticle impregnated MApe, designated as MApe-Mt. The schematic preparation of the composite, as well as its use for BPB adsorption is shown in Scheme 1.

2.3. Adsorbent characterization

The X-ray diffraction (XRD) of the adsorbents was measured by the X-ray diffractometer (Bruker D8-Discover Model) with Cu radiation (λ = 1.54 Å) at step size of 0.1° and counting time of 2 s. The surface functional groups were examined by the Fourier transform infrared spectrometer (FTIR; Brucker Model). The morphology and particle size were also examined with a field emission scanning electron microscope (SEM; Joel JSM-7800F Model) after iridium sputtering on the conductive layer. Elemental composition was determined with an energy dispersive X-ray spectroscopy (EDX, Oxford X-max) coupled to the SEM. The Brunauer-Emmett-Teller surface area (S_{BET}) and pore properties of the adsorbents were analyzed by the surface area and porosity analyzer (Micromeritics ASAP 2020 model) and the results were evaluated by MicroActive VI.01 software. Thermal behavior was examined by the thermo-gravimetric analyzer (TGA; Mettler Toledo Model) at 200 mL/min nitrogen flow rate and 10 °C/min heating time. The pH point of zero charge (pHpzc) was determined by the pH drift method (Jiao et al., 2017).

2.4. Biosorption experiments

An appropriate amount (25.0 mg) of BPB dye was dissolved with distilled water in a 250 mL volumetric flask to prepare a stock solution of concentration 100 mg/L. Further concentrations of 10–50 mg/L were prepared from the stock by dilution. The pH of these solutions were adjusted to a range of 2.0–9.0, using 0.1 M HCl or 0.1 M NaOH respectively. Biosorption was conducted by the batch technique; using 0.1 g of adsorbent with 10 mL of 50 mg/L BPB contaminated solution. The mixture was agitated for 5 min and left for a contact time of 240 min. The solution was then centrifuged at 8000 rpm for 25 min and the filtrate analyzed for residual BPB with the UV spectrophotometer (Shimadzu UV-1800 model), at a wavelength of 590 nm. The effect of varying pH (2.0–9.0), contact time (10–240 min), BPB concentration (10–50 mg/L), Temperature (300–323 K) and biosorbent dosage (0.02–0.10 g) was evaluated. The respective studied parameter was varied while maintaining the others constant. Each exper-

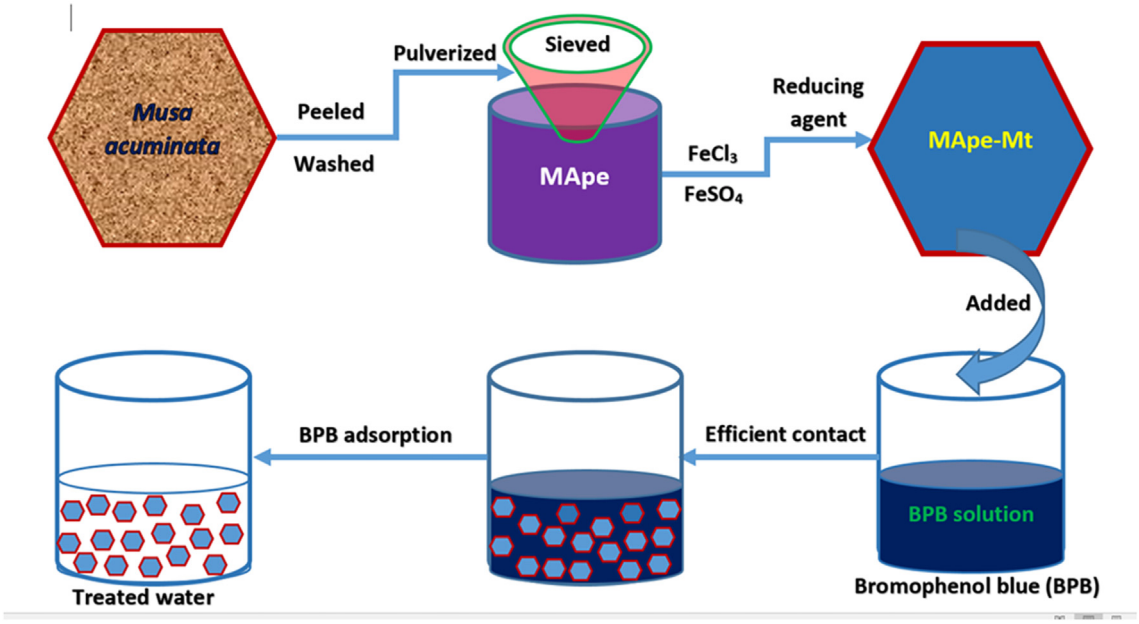

Scheme 1 Preparation of the ferrimagnetic Magnetite (Fe_3O_4) nanoparticle impregnated *Musa acuminata* banana peel composite (MApe-Mt) and its application for the adsorption of bromophenol blue from waste solution.

iment was performed in duplicate and the mean calculated for quality assurance. The uptake capacity (qe, mg/g) and percentage removal (R%) were calculated from the following equations respectively (Ezekoye et al., 2020).

$$qe = [(C_o - C_e)v]/m \quad (1)$$

$$R(\%) = [(C_o - C_e)/C_o]100 \quad (2)$$

Where m (g) is the adsorbent weight, v (L) is the volume of solution; C_o and C_e in mg/L are the initial and equilibrium BPB concentrations respectively.

2.5. Regeneration and reusability

The regeneration of the adsorbents was performed using 0.5 M NaOH solution as eluent. Here, 0.1 g of BPB loaded adsorbent was added to 10 mL of the 0.5 M NaOH eluent, the mixture was agitated for 10 min, then left for a contact time of 30 min. The amount of BPB desorbed into the eluent solution was determined by the UV spectrophotometer. The regenerated adsorbent was oven dried at 80 °C for 30 min, then reused for dye adsorption at a BPB concentration of 50 mg/L, pH 4.0 and contact time of 240 min. Three cycles of regeneration and reuse of the same adsorbent material was carried out to evaluate the potential recycling of both MApe and MApe-Mt. The experiments were performed in duplicate and mean values were computed.

2.6. Statistical analysis

The fitting of the kinetic and isotherm models applied in the description of adsorption, were described by the coefficient of determination (R^2) and sum of square errors (SSE). The larger the R^2 value and the smaller the SSE, the better the model fitting. The SSE is expressed as follows (Foo and Hameed, 2010):

$$SSE = \sum \left(qe_{cal} - qe_{exp}\right)^2 \quad (3)$$

where qe_{cal} and qe_{exp} in mg/g denote the calculated model and experimental uptake capacity respectively. The R^2 and SSE values were estimated by the statistical function of the Origin 2019b software.

3. Results and discussion

3.1. Characterization of MApe and MApe-Mt

The surface functional groups on MApe and MApe-Mt were examined by the FTIR analysis, as shown in Fig. 1a. As indicated for pristine MApe, OH stretching was depicted at 3327 cm^{-1}, while C-H stretching was observed at 2942 cm^{-1} (Chukwuemeka-Okorie et al., 2018). Alkyne bands were observed at 2153 cm^{-1} and 2003 cm^{-1}, while the absorptions at 1608 cm^{-1}, 1376 cm^{-1} and 1053 cm^{-1} corresponded to the C═O, C═C and C─O functional groups respectively (Trinh et al., 2020). After the impregnation of Mt nanoparticles on MApe , shifts in the absorption bands from 3327 to 3336 cm^{-1} (OH), 1608 to 1624 cm^{-1} (C═O), 1376 to 1371 cm^{-1} (C═C) and 1053 to 1045 cm^{-1} (C─O) were observed. This indicated that Mt impregnation had occurred on these functional sites. Apart from this, a decrease in intensity of these absorption bands was noticed after Mt impregnation, suggesting the occupation of these sites by the Mt NPs. The occurrence of several functional groups on the surfaces of MApe and MApe-Mt as identified by FTIR, indicates the potential of both these biosorbents to interact with the contaminant BPB molecules in solution.

The XRD spectra of MApe and MApe-Mt are shown in Fig. 1b. The diffraction pattern of the pristine MApe showed the presence of KCl. This is evident by diffraction peaks at 2θ values of 28.3°, 40.6°, 50.2°, 58.7°, 66.3° and 73.7°, corresponding to the face-centered KCl cubic structural planes (200), (220), (222), (400), (420) and (422), respectively (Blanton et al., 1995). Similar composition was also reported in the diffraction pattern of MApe by another study (Stavrinou et al., 2018). For the composite MApe-Mt, the appearance of new characteristic magnetite diffractions at 2θ values of 30.4°, 35.3°, 43.2°, 53.3°, 57.1°, 62.5° and 73.9° were observed, corresponding to the seven structural magnetite planes of (220), (311), (400), (422), (511), (440) and (444), respectively (Haldorai et al., 2015). The fact that the Mt diffraction peaks were absent in pristine MApe, confirms the successful impregnation of Mt onto MApe in the hybrid adsorbent. Similar Mt diffraction peaks in other magnetite impregnated composites have also been reported by other studies (Nsom et al., 2019; Rajput et al., 2016). From the main Mt characteristic XRD peak at 2θ (35.3°), the average crystalline Mt size was calculated from the Debye-Scherrer equations, as 21.13 nm. In addition, the XRD composition of the adsorbents was also supported by the EDX results, as shown in Fig. 2. EDX percentage weight compositions of C (59.3), O (33.4), K (5.5), Cl (0.5) and Mg (0.2) were obtained for pristine MApe, while C (52.6), O (28.4), Fe (16.2), K (1.8), Si (0.6) and Cl (0.3) were recorded for composite MApe-Mt. This composition clearly corroborates the presence of Mt on the hybrid adsorbent.

The thermal behaviour of MApe and MApe-Mt was evaluated by the TGA, as shown in Fig. 1c. Both adsorbents showed significant weight loss from around 190 °C to 410 °C, attributed to the moisture removal as well as organic matter decomposition (Eze et al., 2019). The impregnation of Mt increases the thermal stability of MApe, as depicted by the lower weight loss of MApe-Mt with temperature, indicating less decomposition than for pristine MApe. The tendency of Mt nanoparticles to increase the thermal stability of the biosorbent was also observed in another study, in the impregnation of Mt nanoparticles onto pine biomass for the removal of methylene blue dye (Mtshatsheni et al., 2019).

The pHpzc of the adsorbents, as determined from the pH drift method, is shown in Fig. 1d. This parameter is significant as it reveals the surface charge on the adsorbents. The pHpzc of untreated MApe was 6.4, which is close to the previous values of 6.2 (Bhaumik and Mondal, 2016) and 6.54 (Stavrinou et al., 2018) reported for MApe. However, the presence of Mt NPs increased the pHpzc of the biosorbent to 7.2. This increase is desirable as pH < pHpzc, the surface of the adsorbent is positive, thus favoring the adsorption of anionic pollutants such as BPB (Jiao et al., 2017). A higher pHpzc simply implies additional positive surface potential, for increased uptake of BPB, in the pH range of 6.4–7.2 for the composite MApe-Mt.

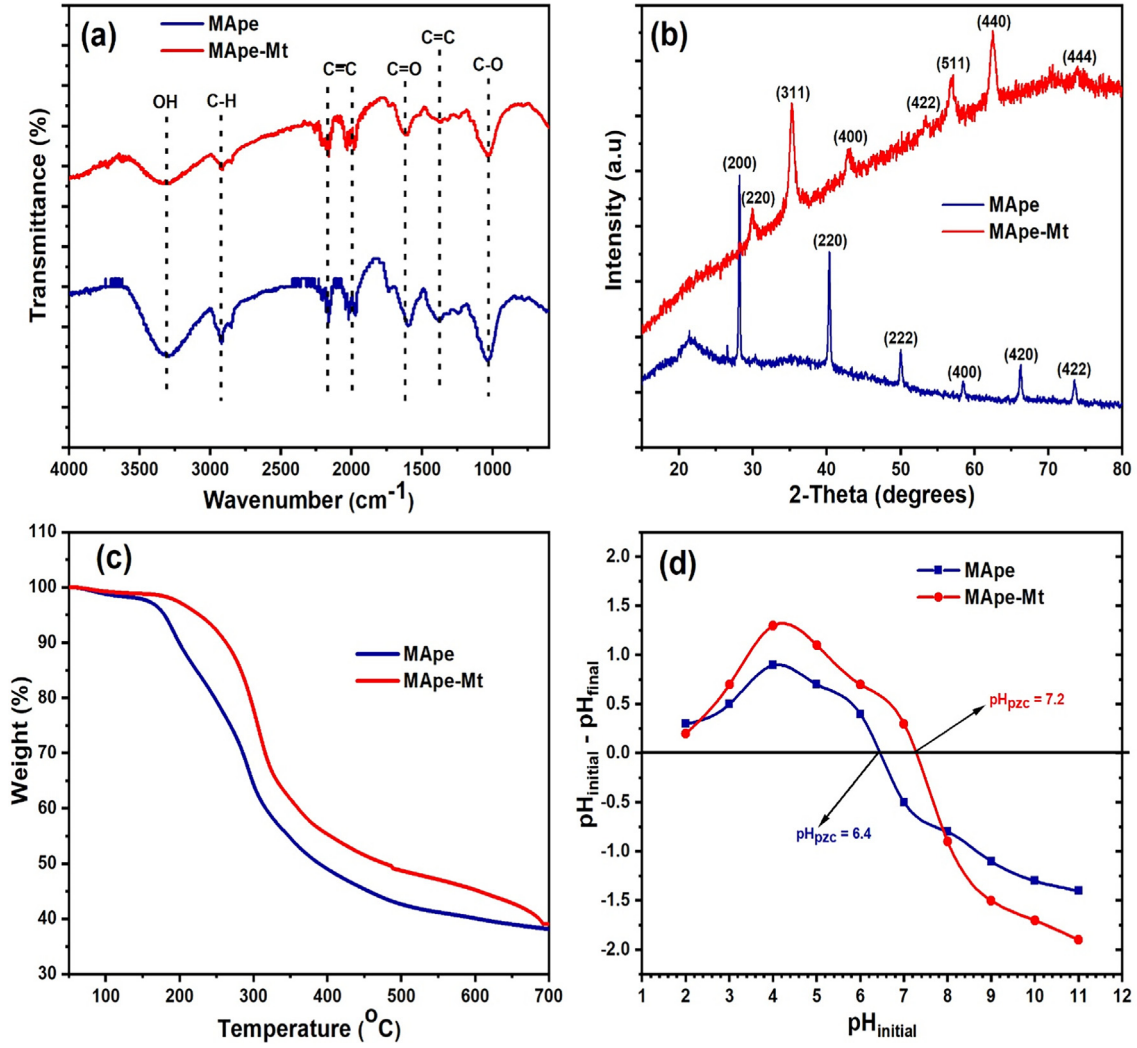

Fig. 1 The (a) Fourier transform infrared spectra, (b) X-ray diffraction (c) Thermogravimetric analysis and (d) pH point of zero charge of MApe and MApe-Mt.

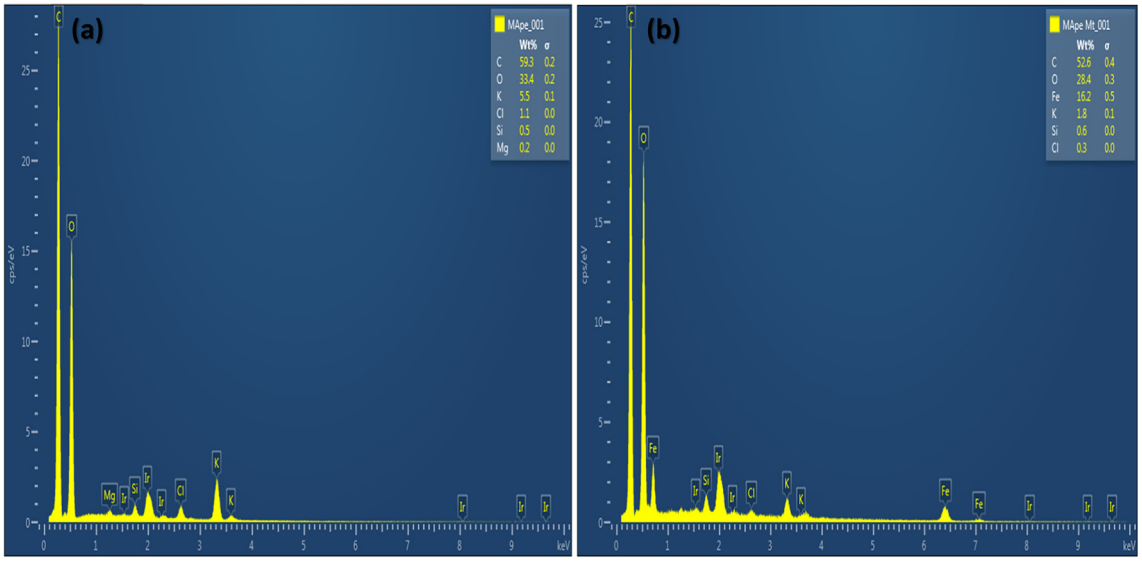

Fig. 2 Energy dispersive X-ray analysis of (a) MApe and (b) MApe-Mt.

The surface area and pore properties of the materials were determined, as illustrated in the N_2 adsorption-desorption isotherm and pore analysis in Fig. 3. The BET surface area (S_{BET}) of MApe was 14.89 m^2/g, while that of MApe-Mt was 3.80 m^2/g. Although, there was a decrease in the S_{BET} of the biosorbent after Mt impregnation, MApe-Mt showed a higher pore volume and pore diameter of 0.01418 cm^3/g and 3.11 nm respectively, compared to 0.00516 cm^3/g and 2.25 nm for MApe. The enhanced pore properties would likely favour the uptake of BPB molecules onto composite MApe-Mt. The lower available surface area could have resulted from the impregnation of Mt particles on the pores of MApe. It is important to mention that the lower surface area does not imply lower adsorption potentials of the adsorbent (Akpomie and Conradie, 2020). In addition, the existence of H3-type hysteresis loop for MApe-Mt, correlating to the type V isotherm according to the IUPAC classification, shows the existence of a mesoporous structure. The mesoporous structure of the adsorbent would allow easy diffusion of dye molecules through the pores for efficient adsorption (Ali et al., 2019d, 2018b).

The surface morphology of MApe and MApe-Mt was revealed in the SEM images presented in Fig. 4. MApe presented an irregular and porous surface structure with particles of different sizes and shapes. There is a clear observation of the presence of Mt nanoparticles on the surface of MApe-Mt after Mt impregnation, which was absent in untreated MApe. In the hybrid, the Mt nanoparticles displayed an agglomerated morphology on the surface of MApe. The average Mt particle size calculated from individual particles was found to be 25.97 nm, which was close to the average crystalline size of 21.13 nm, obtained from the Debye-Scherrer equation.

3.2. Removal dependence on solution pH

The adsorption of dyes is strongly dependent on pH of the wastewater, since the pH influences the surface characteristics of the adsorbent, as well as the ionization and solubility of dyes. The dependence of BPB adsorption onto MApe and MApe-Mt, as a function of solution pH, is illustrated in Fig. 5a. With a pH increase from 2.0 to 9.0, a decrease in the uptake of BPB from 3.6 to 1.9 mg/g for pristine MApe, and from 4.23 to 2.3 mg/g for MApe-Mt, was recorded respectively. A similar decrease in removal from 72.3 to 38.4% and from 86.6 to 46.3% was observed for the respective adsorbents. This indicated that lower pH of the solution was favourable for BPB adsorption, due to the anionic nature of the dye (Akpomie and Conradie, 2020). Similar trend of a steady decrease in adsorption of BPB with increasing pH was also documented in literature (Xiang et al., 2019; You et al., 2006). The lower BPB removal at higher pH could be ascribe to electrostatic repulsion between the anionic BPB molecules in solution, and the increasing negative charge on MApe and MApe-Mt. On the other hand, lower pH led to electrostatic attraction between BPB and positive surface sites of the materials (Khoshsang et al., 2018). The consequences suggested that electrostatic interaction must have played a major part in BPB uptake onto the adsorbents. We conducted our experiment using pH 4.0 rather than the optimum of 2.0, since the latter lower pH rarely occurs in real industrial wastewaters. It is clear that Mt impregnation increased the uptake of BPB dye, at all the pH values evaluated, when compared to the pristine adsorbent. The pHpzc of the materials had a significant influence on the effect of pH in the adsorption of BPB. This is attributed to the fact that at lower pH values than the pHpzc, the material surface is associated with a positive charge, but has a negative charge at higher values than the pHpzc (Dawodu and Akpomie, 2014). It is clear from the pHpzc of both MApe (6.4) and MApe-Mt (7.2) that the latter had a wider range of positive surface characteristics than the former. This positive surface attracted the anionic BPB molecules in solution, thus influencing higher uptake than MApe. The higher pHpzc of MApe-Mt compared to MApe must have influenced the removal of BPB from solution. This result establishes the fact that Mt impregnation was favourable for BPB uptake at various pH values, with the same trend displayed for basic blue (Muhammad et al., 2019) and reactive black 5 dyes (Kyzas et al., 2014).

3.3. Isotherm modeling

The isotherm modeling of BPB adsorption onto MApe and MApe-Mt was evaluated from the data obtained from the

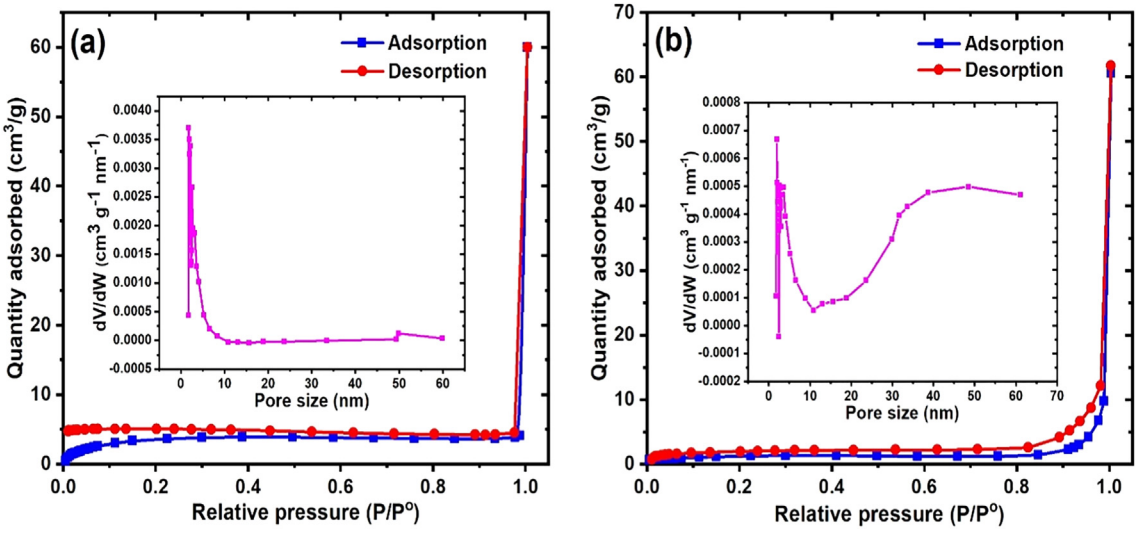

Fig. 3 Nitrogen adsorption-desorption isotherm and pore analysis of (a) MApe and (b) magnetite nanoparticle impregnated MApe-Mt.

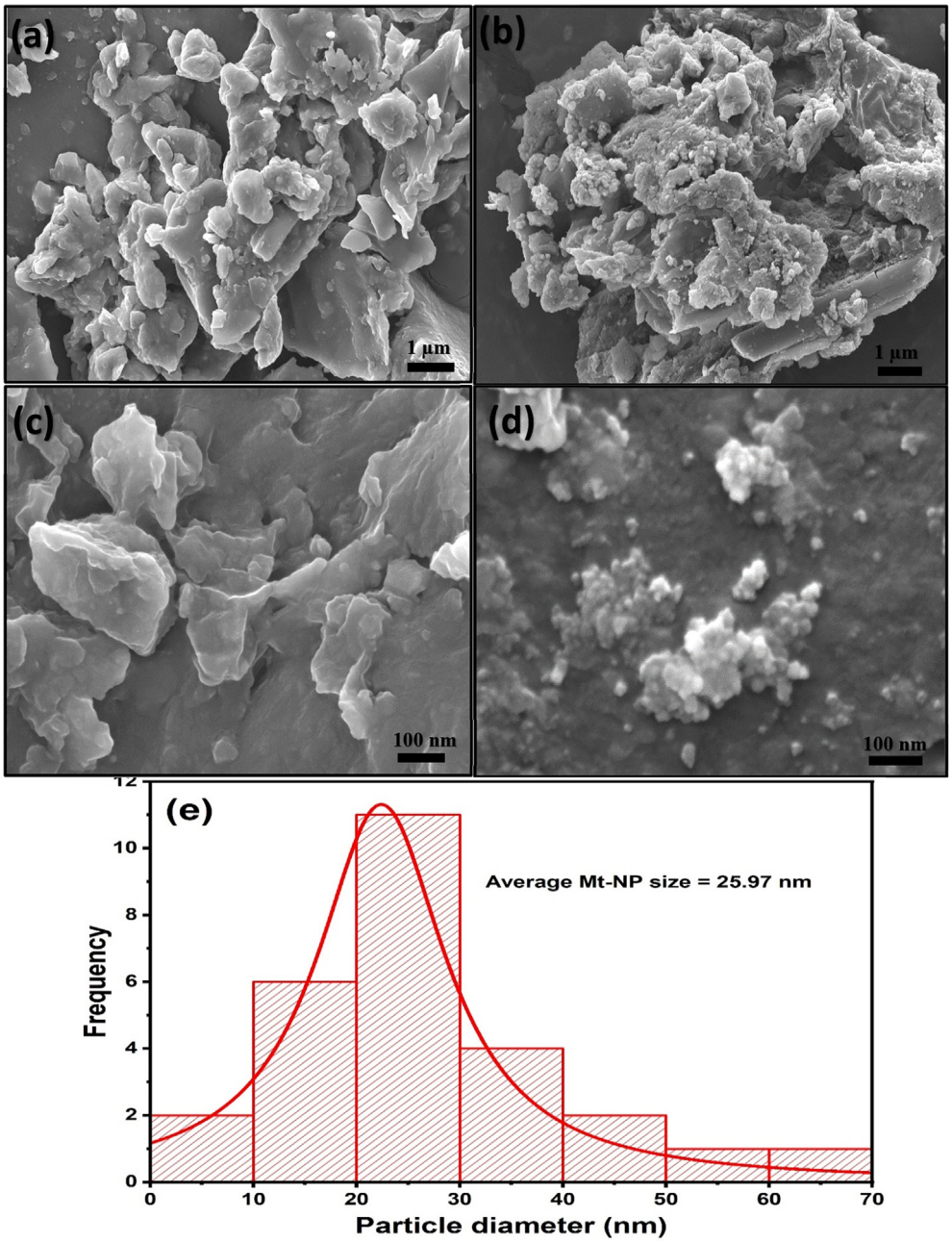

Fig. 4 Scanning electron microscopy of (a, c) MApe and (b, d) MApe-Mt at 1 µm and 100 nm respectively, and (e) particle size distribution of magnetite nanoparticles.

influence of varying BPB concentration on adsorption (Fig. 5b). As depicted, with an increase in BPB concentration from 10 to 50 mg/g, the uptake capacity (qe) increased from 0.8 to 3.3 mg/g and from 0.95 to 4.0 mg/g for MApe and MApe-Mt respectively. This higher uptake is ascribed to greater interaction of BPB dye with the active groups on the surface of the adsorbent materials, resulting from higher dye concentration (Dehmani et al., 2020). On the other hand, we noticed a simultaneous decrease in the overall percentage biosorption from 80.4 to 66.1% and from 95.2 to 80.7% for MApe and MApe-Mt, respectively. This could be since the active sites on the surface of the adsorbents could easily take up BPB from solution at low dye concentration, but eventually become saturated at higher concentrations, leaving more residual BPB behind in solution (Akpomie and Dawodu, 2015a).

The isotherm of biosorption was evaluated by the Freundlich, Langmuir, Temkin and Flory-Huggins isotherm models, with the respective equations given as follows (Foo and Hameed, 2010):

$$log\ qe = log\ K_F + [1/n] log\ C_e \tag{4}$$

$$C_e/qe = 1/q_L K_L + C_e/q_L \tag{5}$$

$$qe = B\ lnA + B\ lnC_e \tag{6}$$

$$log(\theta/C_o) = log\ K_{FH} + n_{FH}\ log(1\ -\ \theta) \tag{7}$$

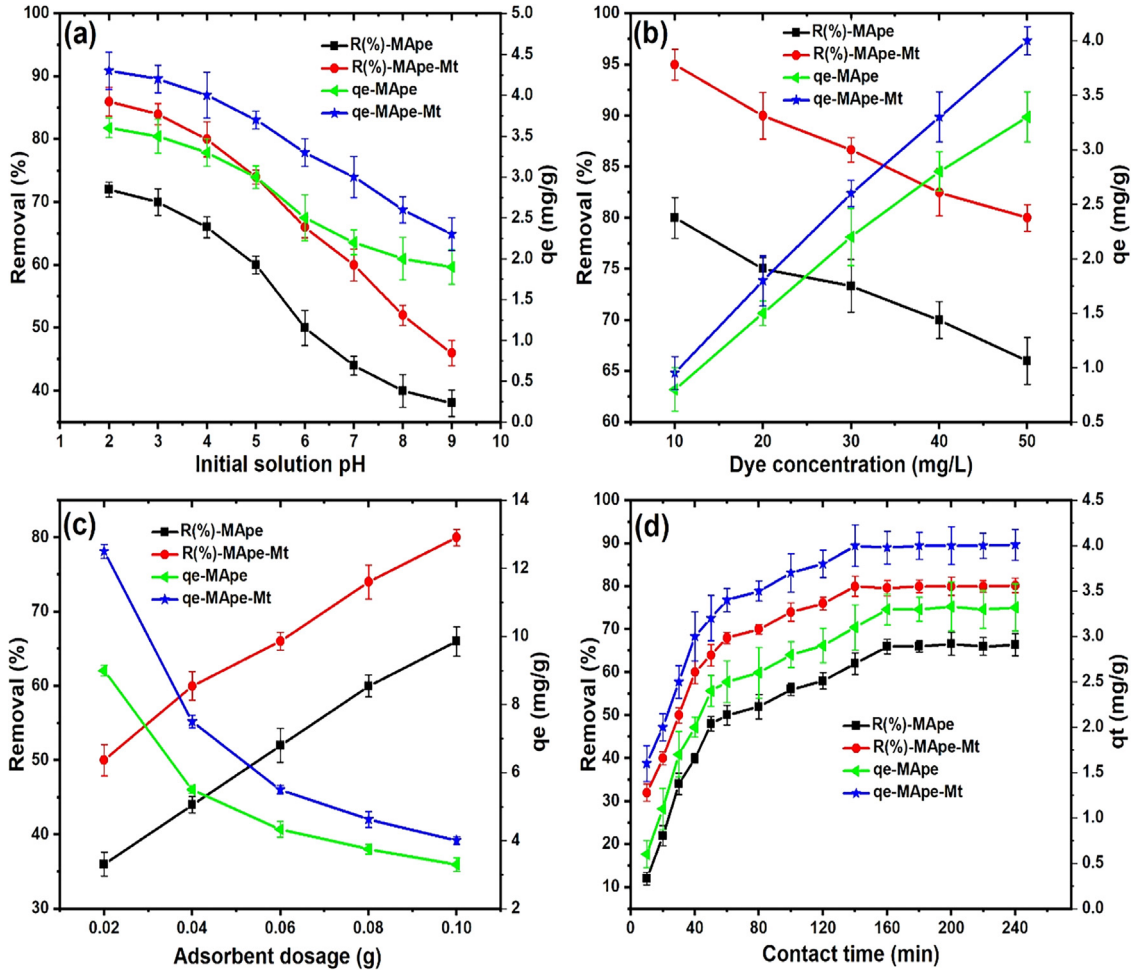

Fig. 5 The influence of (a) pH (dye conc. 50 mg/L, time 240 min, temp 300 K, dosage 0.1 g), (b) Dye concentration (pH 4.0, time 240 min, Temp 300 K, dosage 0.1 g), (c) Adsorbent dosage (pH 4.0, dye conc. 50 mg/L, time 240 min, Temp 300 K), and (d) contact time (pH 4.0, dye conc. 50 mg/L, Temp 300 K, dosage 0.1 g) on BPB uptake onto MApe and MApe-Mt, indicating both uptake capacity qe in mg/g, as well as percentage adsorption for each biosorbent.

The Freundlich adsorption capacity and intensity correspond to n and K_F (L/g) respectively. Langmuir constants are denoted by K_L (L/mg) and q_L (mg/g), while A (L/mg) and B represent the Temkin binding energy and heat of removal, respectively. The constants n_{FH} and K_{FH} are the Flory Huggins model constants, while $\theta = [1 - (C_e/C_o)]$ denotes the adsorbent surface coverage. The isotherm model fittings for BPB uptake onto MApe and MApe-Mt are illustrated in Fig. 6, while the calculated model parameters are presented in Table 1. The Freundlich model clearly gave the best fit to the dye concentration data for both adsorbents, as depicted by the highest R^2 and lowest SSE values. This consequently indicates a multilayer binding of BPB onto the heterogeneous surfaces of MApe and MApe-Mt (Chukwuemeka-Okorie et al., 2018). The heterogeneous surface structure of pristine MApe could be attributed to the presence of both organic components of the biomass, as reflected in the FTIR analysis as well as KCl sites observed in the XRD diffraction. The heterogeneous surface of composite MApe-Mt was also expected, due to the presence of the impregnated Mt sites in addition to the organic sites of MApe to form an inorganic-organic composite. The heterogeneous surface of inorganic-organic composites was also clearly seen in the case of a corn cob-kaolinite combo (Chukwuemeka-Okorie et al., 2018). In that study, a change in the Langmuir fit (homogenous surface) of the individual components (corn-cob and kaolinite) to the Freundlich fit (heterogeneous surface) after their combination was observed (Chukwuemeka-Okorie et al., 2018). A favourable pollutant uptake by any given adsorbent material is indicated by Freundlich n values between 1 and 10 (Ezekoye et al., 2020). The n values obtained from the Freundlich model of 1.48 and 2.09 for MApe and MApe-Mt respectively; therefore confirm efficient binding of BPB onto the surface of both materials. In addition, the Langmuir separation factor R_L was in the range 0.222–0.588 and 0.091–0.333 for MApe and MApe-Mt respectively, therefore for both adsorbents, R_L is less than one, which corroborates the favourable adsorption of BPB (David et al., 2020). The optimum Langmuir monolayer BPB uptake (q_L) for MApe was 6.01 mg/g and for MApe-Mt was 8.12 mg/g. This showed that Mt impregnation slightly increased the uptake of BPB onto MApe. The uptake capacity of MApe and MApe-Mt was compared with other adsorbents applied previously for the adsorption of BPB, as shown in Table 2. Although the prepared adsorbents in this

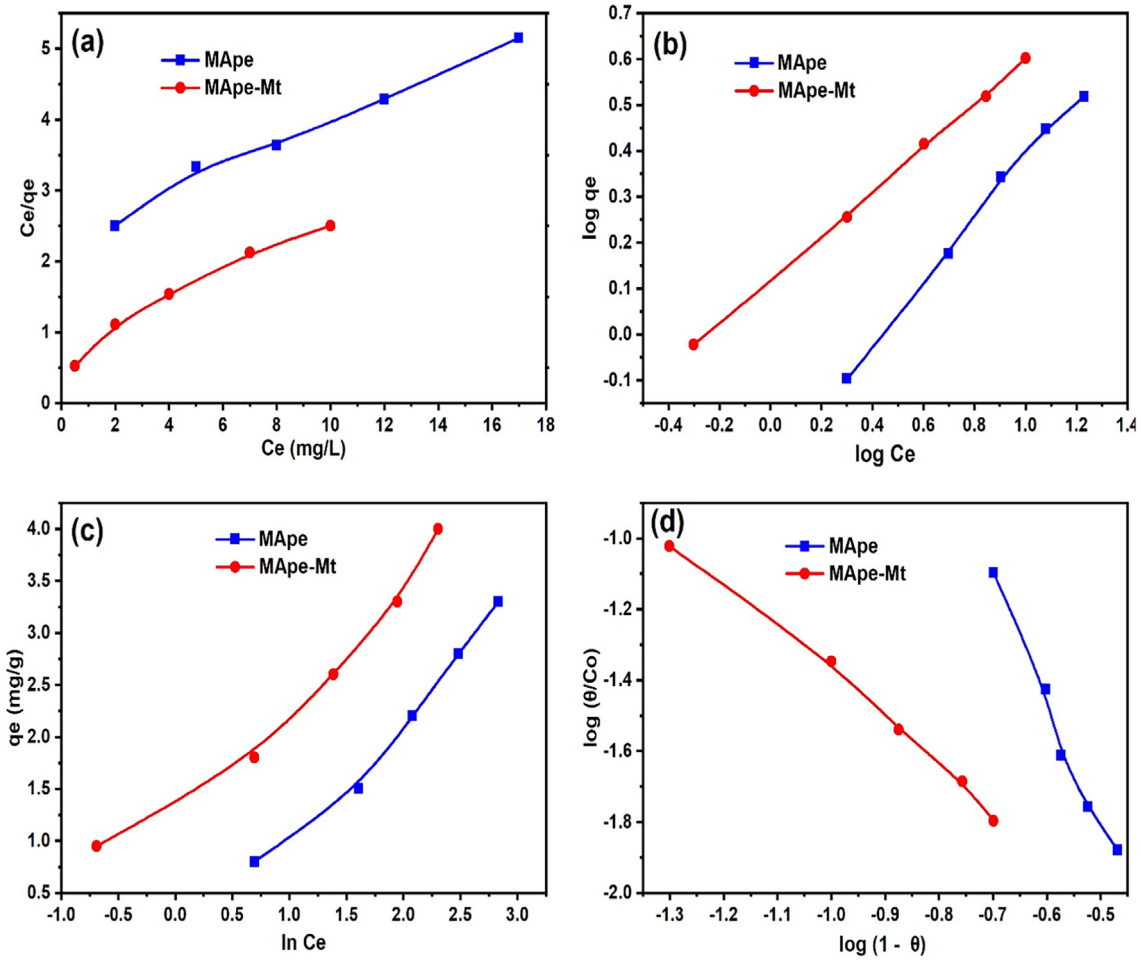

Fig. 6 The (a) Langmuir, (b) Freundlich, (c) Tempkin and (d) Flory Huggins isotherm fittings for the adsorption of bromophenol blue onto MApe and MApe-Mt.

study showed lower uptake than most adsorbents in literature, their adsorption was much higher than polymeric gels (2.99–2.98 mg/g) (Malana et al., 2010) and activated charcoal (0.081 mg/g) (Iqbal and Ashiq, 2007). The uptake onto banana peel bio-materials was also comparable to the polymer-clay composite (10.78 mg/g) (El-Zahhar et al., 2014). The abundant and eco-friendly nature of our prepared adsorbents would be their main advantage for practical application in the treatment of BPB polluted wastewaters.

3.4. Dependence of adsorption on the dosage of MApe and MApe-Mt

The removal of BPB dye from solution onto MApe and MApe-Mt as a function of biosorbent material dosage is shown in Fig. 5c. The adsorption uptake capacity of BPB decreases significantly from 9.0 to 3.3 mg/g and from 12.5 to 4.0 mg/g for the respective adsorbents, with increase in biosorbent dosage from 0.02 to 0.1 g. This is ascribe to the availability of more active sites with dosage increase, for the removal of the same dye concentration (50 mg/L) of BPB, resulting in less amount of dye molecules being adsorbed onto specific active sites. The decrease in uptake capacity is also due to increased collision between biosorbent particles, resulting in aggregation of the active sites as biosorbent dosage is increased (Li et al., 2020). Therefore, maximum utilization of the active sites was not achieved at higher biosorbent dosages. However, the presence of more active sites at higher dosages did result in overall more removal of BPB molecules from solution. With increase in biosorbent dosage from 0.02 to 0.1 g, an increase in the removal of BPB from 36.2 to 66.1% and from 50.6 to 80.7% was obtained for MApe and MApe-Mt respectively. This shows that the uptake capacity reflects the characteristics of the adsorbent material itself, while the percentage removal is associated with the adsorbate or contaminant in solution. Composite MApe-Mt also reflected a higher uptake of BPB than MApe in the dosage range studied, which further supports the suitability of Mt NPs impregnation in enhancing the uptake of dye molecules onto MApe. This trend of decrease in uptake capacity and simultaneous increase in percentage removal with changing dosage, has also been documented by other workers (Jabar and Odusote, 2020; Rai et al., 2016).

3.5. Adsorption kinetics

The kinetics of adsorption is important, as it determines how fast a pollutant is removed from solution. This is vital for economic reasons, as well as in the design of adsorption systems. The effect of contact time on the adsorption of BPB onto

Table 1 Equilibrium isotherm modelling of bromophenol blue adsorption onto both biosorbents MApe and MApe-Mt.

Isotherm	MApe	MApe-Mt
Langmuir		
K_L (L/mg)	0.07	0.2
q_L (mg/g)	6.04	8.12
R^2	0.9858	0.9658
SSE	0.0568	0.0844
Freundlich		
N	1.48	2.09
K_F (L/g)	0.51	1.32
R^2	0.9950	0.9993
SSE	0.0012	0.0002
Tempkin		
B (mg/g)	1.183	0.991
A (L/g)	0.862	4.16
R^2	0.9749	0.9534
SSE	0.1001	0.2698
Flory-Huggins		
K_{FH}	2.759	0.002
n_{FH}	−3.497	−1.2717
R^2	0.9811	0.9926
SSE	0.0071	0.0027

MApe and MApe-Mt is shown in Fig. 5d. It was observed that as the contact time increased from 10 to 240 min, uptake capacity also increased from 0.6 to 3.3 mg/g and from 1.6 to 4.01 mg/g forMApe and MApe-Mt, respectively. A similar increase in percentage BPB removal from 12.1 to 66.2% and from 32.3 to 80.4% was observed for the respective materials. Equilibrium BPB adsorption was achieved at 160 min and 140 min for MApe and MApe-Mt, respectively. This indicated slightly faster kinetics of BPB removal onto the Mt impregnated biosorbent. Apart from that, MApe-Mt also showed higher BPB uptake over the range of contact time studied. The increase in BPB adsorption at the initial stages was ascribed to availability of abundant active sites on the adsorbents, which were eventually used up and saturated, resulting in equilibrium (Akpomie and Dawodu, 2015b; Dhananasekaran et al., 2016), faster for MApe-Mt than for pristine MApe.

The kinetic data modeling was described by the pseudo-first order (PF), pseudo-second order (PS), Film diffusion (FD) and intraparticle diffusion (ID) kinetic models, whose respective equations are given as (Ezekoye et al., 2020):

$$log(qe - qt) = log\ qe - (K_1 t/2.303) \quad (8)$$

$$t/qt = 1/K_2 qe^2 + t/qe \quad (9)$$

$$ln(1 - F) = Y - K_{FD} t \quad (10)$$

$$qt = K_d t^{1/2} + C \quad (11)$$

The constant F depicts fractional equilibrium attainment, while K_d, K_{FD}, K_2 and K_1 are the rate constants of the ID, FD, PS and PF kinetic data models, respectively. The qt (mg/g) represents the uptake capacity at time (t), while Y and C correspond to the intercept of the FD and ID equations, respectively. The kinetic model fittings for BPB adsorption are shown in Fig. 7, while the calculated kinetic parameters are presented in Table 3. Although the PS gave a higher R^2 than the PF kinetic model, there was great discrepancy between the theoretical and experimental qt values for PS, as revealed by the high SSE for the PS kinetic model. In addition, the calculated qe (qe_{cal}) values of the PF model were very close to the experimental qe (qe_{exp}) uptake capacity, more than for the PS model. This clearly depicts that the PF model best describes the uptake of BPB onto MApe and MApe-Mt and that chemisorption therefore is not the rate controlling mechanism (Olu-Owolabi et al., 2012). In addition, the rate constant of the PF model of 0.026 min^{-1} for the composite MApe-Mt was higher than the rate constant of 0.0234 min^{-1} obtained for untreated MApe. Similarly, a higher PS rate constant was also obtained for composite MApe-Mt. This result corroborates the faster equilibrium uptake of BPB onto MApe-Mt compared to MApe, obtained from the variation in contact time. Faster equilibrium uptake is desired in adsorption systems for practical application in industrial wastewater treatment, as time is saved in the treatment process. Furthermore, the higher R^2 and lower SSE presented by the FD compared to the ID kinetic data model, showed that film diffusion was

Table 2 Comparison of the prepared adsorbents with other adsorbents applied for bromophenol blue adsorption.

Adsorbent	pH	Dosage (g)	Conc (mg/L)	Time (min)	qe (mg/g)	References
Activated charcoal	1.0–7.0	0.01	6.7	60	0.081	(Iqbal and Ashiq, 2007)
Polymeric gels	7.0	0.5	1–11	300	2.984	(Malana et al., 2010)
MApe	4.0	0.1	50	240	6.04	This study
MApe-Mt	4.0	0.1	50	240	8.12	This study
Polymer-clay composite	–	0.15	50	60	10.78	(El-Zahhar et al., 2014)
Sorel cement nanoparticles	8.3	0.05– 0.25	2.84– 25.14	90	16.39	(El-Gamal et al., 2015)
Mesoporous hybrid gel	3.0	0.125	0.02 mM	12,000	17.67	(You et al., 2006)
Graphene oxide	7.0	0.01	15	10	17.94	(Fathy et al., 2019)
Chitin nanoparticles	6.0	0.015	15	50	22.72	(Dhananasekaran et al., 2016)
Biomass derived activated carbon	1.0	1.0	10	50	23.45	(Ghaedi et al., 2014)
CuS-activated carbon composite	7.0	0.0091	10	10	106.38	(Mazaheri et al., 2016)
Supported ionic liquid	2.0–7.0	0.01	10–70	30	217.39	(Liu et al., 2014)

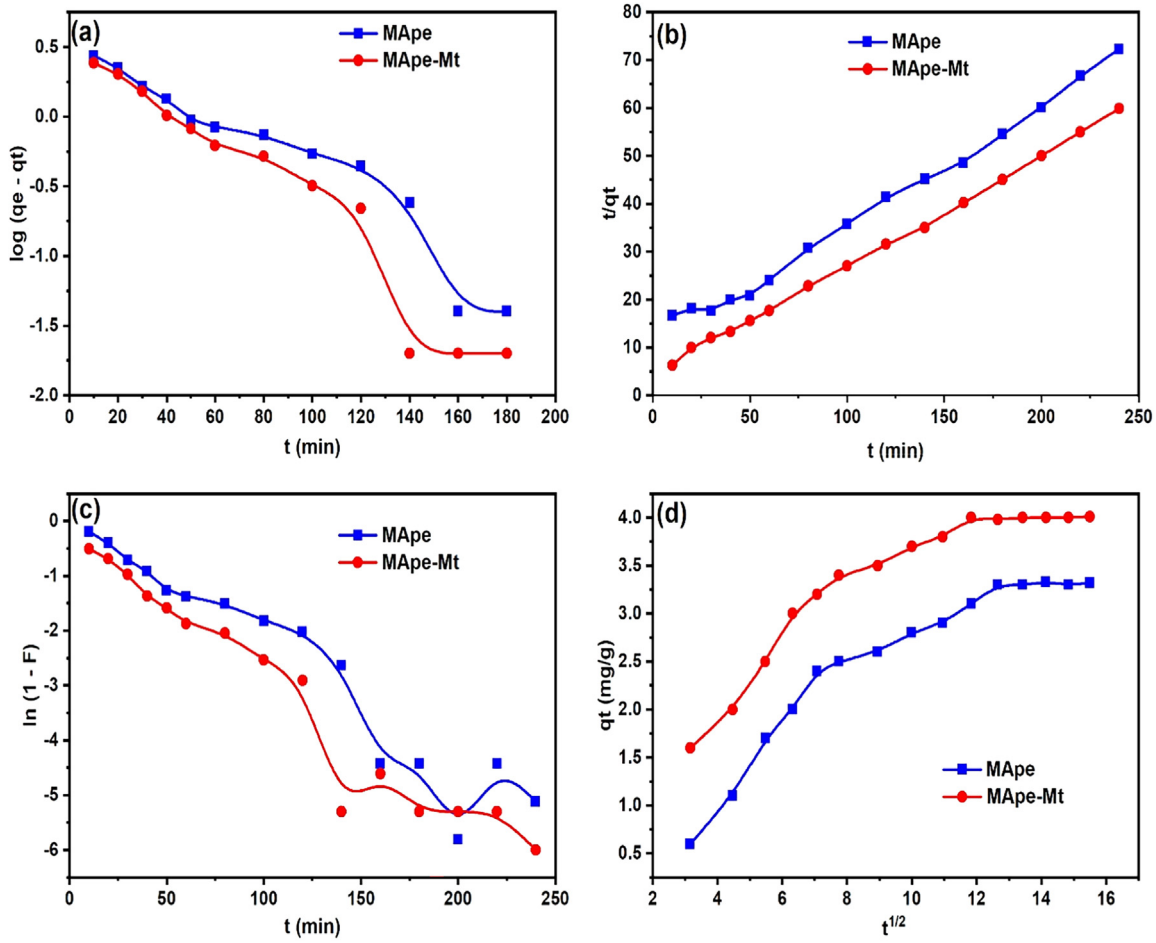

Fig. 7 The (a) Pseudo-first order, (b) Pseudo-second order, (c) Film diffusion and (d) Intraparticle diffusion kinetic fittings for the adsorption of bromophenol blue onto MApe (blue) and MApe-Mt (red), where qe (in mg/g) is the uptake capacity, constant F depicts fractional equilibrium attainment, and qt represents the uptake capacity at time (t).

the major diffusion mechanism of BPB removal onto MApe and MApe-Mt (Chukwuemeka-Okorie et al., 2018). This film diffusion mechanism must have played a major role, since the contact between BPB dye and the adsorbents was mostly carried out under settled conditions rather than with continuous agitation of the system. The intraparticle diffusion mechanism (ID) is usually dominant in a well-agitated adsorption system, which promotes efficient diffusion of the dye adsorbate from the surface to the interior surface sites of the adsorbent (Akpomie et al., 2018).

3.6. Thermodynamics of BPB uptake

The characteristic temperature effect on effective BPB uptake onto MApe and MApe-Mt was also examined. There was a slight increase in BPB uptake from 3.3 to 3.77 mg/g and from 4.1 to 4.33 mg/g onto MApe and MApe-Mt, respectively, with increasing solution temperature from 300 to 323 K. In addition, an increase in percentage removal from 66.1 to 75.4% and from 80.6 to 86.6% was also recorded for the respective adsorbents. A similar increase in adsorption of other dyes onto Mt impregnated adsorbents with increased temperature, have also been observed (Kyzas et al., 2014; Yadav et al., 2020).

The thermodynamic perspective of adsorption was examined, by considering the changes in free energy (ΔG^o), enthalpy (ΔH^o) and entropy (ΔS^o) for the adsorption process, as obtained from the following equations (Nassar et al., 2017; Shang et al., 2019):

$$\Delta G^o = -RT\ ln\ K_c \tag{12}$$

$$ln\ K_c = -\ (\Delta H^o/RT) + (\Delta S^o/R) \tag{13}$$

Where K_c (C_a/C_e) is the equilibrium constant, and C_a (mg/L) = $C_o - C_e$, is the concentration of BPB adsorbed from solution onto the biosorbent at equilibrium, T (K) is the sorption temperature and R (J/molK) is the universal constant. The thermodynamic parameters of the BPB adsorption onto both MApe and MApe-Mt are presented in Table 4. A feasible and spontaneous uptake of BPB dye onto the biosorbent materials was indicated by the negative ΔG^o values (Mohammed et al., 2020; Nassar et al., 2018). The increase in negativity of ΔG^o with temperature also suggested that higher temperature was favourable for BPB uptake (Nassar et al., 2019). An increase in collisions between the BPB in solution and the surfaces of MApe and MApe-Mt with increased temperature was revealed by positive ΔS^o values (Shakoor and Nasar, 2016). In

Table 3 Kinetic modelling of bromophenol blue adsorption onto MApe and MApe-Mt.

Kinetic model	MApe	MApe-Mt
qe_{exp} (mg/g)	3.33	3.98
Pseudo-first order		
K_1 (min^{-1})	0.0234	0.026
qe_{cal} (mg/g)	3.71	3.85
R^2	0.9213	0.9330
SSE	0.7245	0.5775
Pseudo-second order		
K_2 (g/mg min)	0.0056	0.0118
qe_{cal} (mg/g)	4.04	4.39
R^2	0.9925	0.9988
SSE	37.829	5.2711
Intraparticle diffusion		
K_d (mg/g $min^{-1/2}$)	0.2042	0.1818
C	0.5556	1.6032
R^2	0.8829	0.8403
SSE	1.2092	1.3754
Film diffusion		
K_{fd}	0.0234	0.0252
Y	0.1050	0.3124
R^2	0.9213	0.9482
SSE	1.1236	1.0217

addition, the endothermic nature of BPB uptake onto the materials was affirmed by positive ΔH^o values recorded for both materials. The physical adsorption of BPB onto the biosorbent materials which was deduced from the PF kinetic evaluation, was further corroborated by ΔH^o values within the range 2.1 to 20.9 kJ/mol (Ogbu et al., 2019). This physisorption mechanism suggests that weak forces of attraction between BPB and the surface functionality of both MApe and MApe-Mt must have played a major role in the overall adsorption process (Feiqiang et al., 2018). Easy regeneration of our prepared materials is therefore likely to be achieved, due to the physical nature of interactions between the BPB contaminant and the adsorbents.

3.7. Effect of competing metal ions

The effect of competing heavy metal ions on the adsorption of BPB onto MApe and MApe-Mt was evaluated. This was carried out because dye industrial effluents generally also contain significant amounts of heavy metal ions, which could interfere with the uptake of dye onto the adsorbents. Four heavy metals commonly found in effluents were selected for this study, namely Pb(II), Ni(II), Cd(II) and Zn(II) and their influence on the BPB uptake onto the prepared adsorbents was investigated. In this study, solutions containing 50 mg/L BPB and 50 mg/L of each heavy metal ion were prepared, to ensure an equal concentration of dye and heavy metal in solution. Ten milliliters of each binary component solution at pH 4.0 was added to 0.1 g of each adsorbent material, agitated for 5 min and left for a contact time of 240 min at 300 K. The residual BPB concentration in the filtrate was determined after separation of the saturated adsorbent from solution. Fig. 8 shows the influence of the heavy metal ions on the percentage uptake of BPB by the adsorbents. The presence of Zn(II) and Cd(II) in solution only had a slight decrease in the removal of BPB by the adsorbents, while Ni(II) and Pb(II) had a more significant decrease. This suggests that both MApe and MApe-Mt had higher affinity for Ni(II) and Pb(II) ions compared to Zn(II) and Cd(II). Thus, Ni(II) and Pb(II) were more effectively adsorbed onto the active sites, causing a decrease in the number of sites available for further BPB removal from solution. Interestingly, this trend was strongly related to the hydrated ionic radius of each metal ion (with the smallest ionic radius being best adsorbed): Pb (0.401 nm) < Ni (0.404 n m) < Cd (0.426) < Zn (0.43 nm) and also related to the electronegativity of the metal (with the highest electronegativity being best adsorbed): Pb (2.33) > Ni (1.91) > Cd (1.69) > Zn (1.65). Thus, Pb(II) and Ni(II) had smaller ionic radii for easy diffusion and interaction, as well as higher electronegativity for attraction to the functional groups on the surface of the adsorbents (Chukwuemeka-Okorie et al., 2018). The fact that a significant amount of BPB dye was still removed from solution in the presence of the metal ions, showed the viability of these adsorbents for BPB adsorption. This although the pH used was lower than the pHpzc of both adsorbents, indicating a positive adsorbent surface for attraction of the anionic BPB dye and simultaneous repulsion of cationic heavy metal ions (Dawodu and Akpomie, 2014). In general, the binding of metal ions onto the MApe and MApe-Mt adsorbents, decreases the active sites available for the removal of BPB. It is important to note that MApe-Mt still showed higher BPB uptake than pristine MApe, even in the presence of the heavy metal ions in solution, suggesting the efficiency of Mt impregnation in enhancing the uptake of BPB onto the composite adsorbent.

3.8. Adsorption mechanism

The mechanism of BPB adsorption onto MApe and MApe-Mt was elucidated from the FTIR analysis of the adsorbents before and after the adsorption of BPB. This is significant as shifts in adsorption bands of the materials after adsorption

Table 4 Thermodynamic analysis of bromophenol blue adsorption onto MApe and MApe-Mt.

Adsorbent	T(K)	K_c	ΔG^o (kJ/mol)	ΔH^o (kJ/mol)	ΔS^o (J/mol K)	R^2
MApe	300	1.94	−1.65	15.867	58.33	0.9925
	313	2.44	−2.33			
	323	3.06	−3.01			
MApe-Mt	300	4.00	−3.46	16.494	66.32	0.9631
	313	4.88	−4.13			
	323	6.46	−5.01			

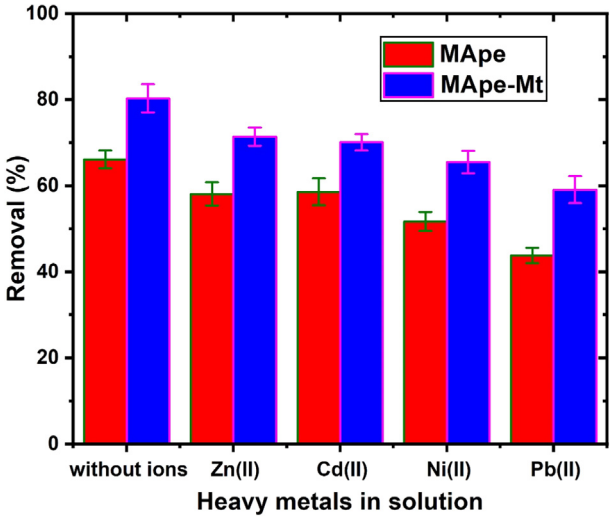

Fig. 8 Effect of competing heavy metal ions in solution on the percentage adsorption of bromophenol blue onto both adsorbents MApe and MApe-Mt.

help to identify the surface functional groups responsible for the adsorption of the dye (An et al., 2020a). The FTIR spectra of MApe before and after BPB uptake is shown in Fig. 9a. We observed significant shifts after adsorption in the OH bands from 3327 to 3354 cm^{-1}, the C═O bands from 1608 to 1625 cm^{-1}, the C-O stretching from 1053 to 1031 cm^{-1}, while the C-H and C═C were relatively unchanged. This indicates that the OH, C═O and C-O functional groups of MApe were responsible for BPB adsorption by interaction with the BPB molecules in solution. Similarly, from Fig. 9b, shifts in the absorption bands of MApe-Mt from 3336 to 3295 cm^{-1}, 1624 to 1621 cm^{-1} and 1645 to 1640 cm^{-1} for OH, C═O and C-O respectively, showed that these functional moieties were responsible for the uptake of BPB onto MApe-Mt. It has been stated previously that the OH, NH and C═O functional groups are mainly responsible for the adsorption of pollutants onto biosorbents (Rajapaksha et al., 2016). It is clear that Mt impregnation on the pristine adsorbent did not alter the active surface sites responsible for BPB uptake. The involvement of the hydroxyl and carboxyl functionalities suggests possible uptake of BPB dye onto the adsorbent by H-bonding and hydrophobic as well as electrostatic interactions (Şenol, 2020; Singh et al., 2020b).

3.9. Recycling of MApe and MApe-Mt

The recycling of adsorbents by efficient regeneration and reuse is important for economic applications and avoidance of

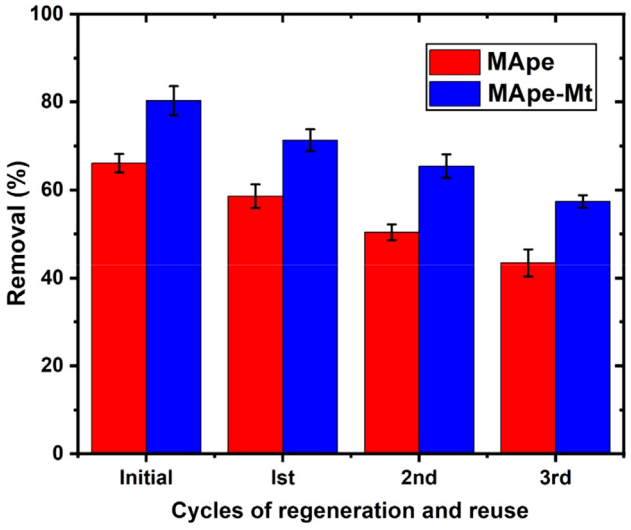

Fig. 10 Adsorption-desorption regeneration cycles for the repeated adsorption of bromophenol blue onto MApe and MApe-Mt.

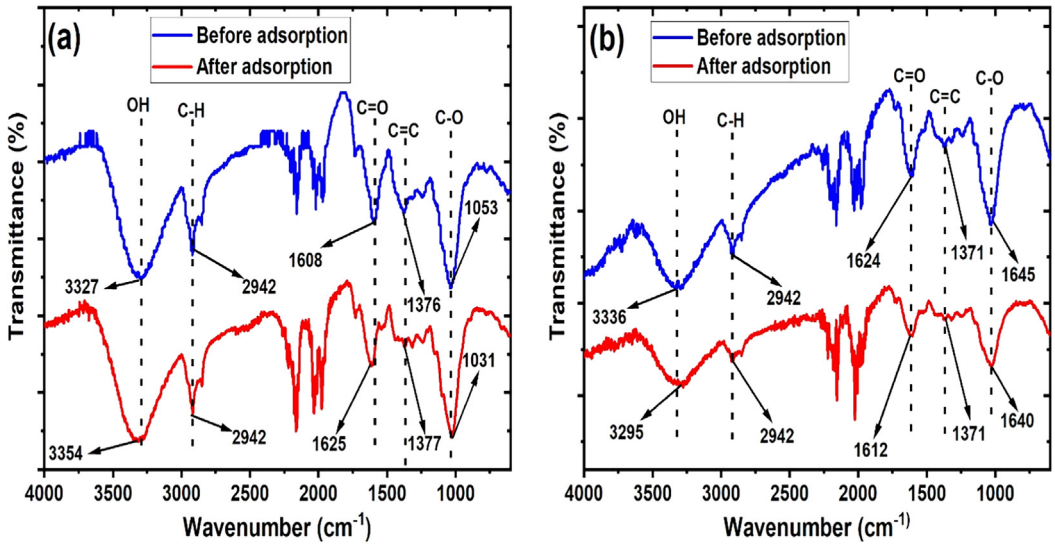

Fig. 9 Fourier transform infrared spectra of biosorbents (a) MApe and (b) MApe-Mt, both before and after the adsorption of bromophenol blue, indicating which active sites had been used for biosorption of the dye.

secondary contamination (Chatterjee and Abraham, 2019; Momina et al., 2018). The regeneration of these adsorbents using alkaline solution as stripping agent, showed 90.6% and 92.3% desorption of BPB from the loaded MApe and MApe-Mt, respectively. This high desorption percentage is desirable and suggests easy regeneration of the materials, which is attributed to the physical nature of BPB bonding onto the adsorbents. In addition, three successive cycles of reuse as shown in Fig. 10, presented a gradual decrease in percentage BPB removal, from 66.1 to 43.4% onto MApe and from 80.3 to 57.4% onto MApe-Mt, respectively. This decrease could be attributed to weight loss of the biosorbent materials, incomplete desorption from the functional groups before reuse, as well as alterations of the active sites, due to the destructive effect of the desorbing agent (Nessim et al., 2011). Irrespective of these factors, both adsorbents showed efficient potential for recycling. In addition, the spent adsorbents obtained after extended reuse, could be applied as biofuels and as additives in the manufacturing of building materials (Mohanta and Ahmaruzzaman, 2018).

4. Conclusions

In conclusion, magnetite (Mt) nanoparticle impregnated *Musa acuminata* bio-waste (MApe-Mt) was synthesized in a one-pot system and successfully applied for the adsorption of bromophenol blue (BPB) dye. The uptake of BPB onto *Musa acuminata* waste (MApe) was enhanced by the impregnation of Mt nanoparticles (ferromagnetic Fe_3O_4) onto MApe. Experimental variables such as temperature, pH, adsorbent dosage, contact time and dye concentration, influenced the overall removal of BPB. Higher dye adsorption was recorded onto the MApe-Mt composite compared to pristine MApe, for all variations in the above operating conditions. The FTIR analysis showed the hydroxyl and carbonyl groups as the major functional sites for BPB adsorption onto both MApe and MApe-Mt. The impregnation of Mt nanoparticles onto MApe increased the pore properties, pH point of zero charge, as well as the thermal stability of the adsorbent, while XRD, EDX and SEM characterizations showed successful impregnation of 25.97 nm (average) sized Mt particles onto MApe-Mt. Although the Mt impregnation decreased the surface area of the adsorbent, yet the MApe-Mt composite recorded a higher monolayer uptake capacity of 8.12 mg/g, compared to 6.04 mg/g obtained for the pristine MApe. The effect of co-existing heavy metal ions in the contaminated solution showed only a slight decrease in BPB uptake in the presence of Zn(II) and Cd(II), with a more significant decrease when Ni(II) and Pb(II) were present, with smaller ionic radius and higher electronegativity. The Freundlich isotherm model was well fitted to the adsorption of BPB dye onto both adsorbents, which indicated heterogeneous material surfaces involving multilayer BPB binding. The kinetic data was well fitted by the liquid film and pseudo-first order equation. A spontaneous, endothermic and physical adsorption of BPB onto MApe and MApe-Mt was deduced from thermodynamic evaluation. This physisorption enabled easy regeneration (over 90% BPB desorption) and reusability of both MApe and MApe-Mt. These results proved the viability of the prepared biosorbents for efficient treatment of BPB polluted water, with Mt nanoparticles enhancing the adsorption of potential of the bio-waste.

Acknowledgement

The authors are grateful to the University of the Free State, South Africa, for the financial support to conduct this research.

References

Abdel-Ghani, N.T., El-Chaghaby, G.A., Rawash, E.-S.-A., Lima, E. C., 2019. Magnetic activated carbon nanocomposite from Nigella sativa L. waste (MNSA) for the removal of Coomassie brilliant blue dye from aqueous solution: Statistical design of experiments for optimization of the adsorption conditions. J. Adv. Res. 17, 55–63.

Aguayo-Villarreal, I.A., Cortes-Arriagada, D., Rojas-Mayorga, C. K., Pineda-Urbina, K., Muñiz-Valencia, R., González, J., 2020. Importance of the interaction adsorbent –adsorbate in the dyes adsorption process and DFT modeling. J. Mol. Struct. 1203, 127398. https://doi.org/10.1016/j.molstruc.2019.127398.

Ahmad, T., Danish, M., 2018. Prospects of banana waste utilization in wastewater treatment: A review. J. Environ. Manage. 206, 330–348.

Akpomie, K.G., Conradie, J., 2020. Banana peel as a biosorbent for the decontamination of water pollutants. A review. Environ. Chem. Lett. https://doi.org/10.1007/s10311-020-00995-x.

Akpomie, K.G., Dawodu, F.A., 2015a. Montmorillonite-rice husk composite for heavy metal sequestration from binary aqua media: A novel adsorbent. Trans. R. Soc. South Africa 70, 83–88.

Akpomie, K.G., Dawodu, F.A., 2015b. Physicochemical analysis of automobile effluent before and after treatment with an alkaline-activated montmorillonite. J. Taibah Univ. Sci. 9, 465–476.

Akpomie, K.G., Dawodu, F.A., Eze, S.I., Asegbeloyin, J.N., Ani, J. U., 2018. Heavy metal remediation from automobile effluent by thermally treated montmorillonite-rice husk composite. Trans. R. Soc. South Africa 73, 254–263.

Ali, I., Peng, C., Khan, Z.M., Naz, I., Sultan, M., 2018a. An overview of heavy metal removal from wastewater using magnetotactic bacteria. J. Chem. Technol. Biotechnol. 93, 2817–2832.

Ali, I., Peng, C., Khan, Z.M., Naz, I., Sultan, M., Ali, M., Abbasi, I. A., Islam, T., Ye, T., 2019a. Overview of microbes based fabricated biogenic nanoparticles for water and wastewater treatment. J. Environ. Manage. 230, 128–150.

Ali, I., Peng, C., Khan, Z.M., Sultan, M., Naz, I., 2018b. Green Synthesis of Phytogenic Magnetic Nanoparticles and Their Applications in the Adsorptive Removal of Crystal Violet from Aqueous Solution. Arab. J. Sci. Eng. 43, 6245–6259.

Ali, I., Peng, C., Lin, D., Naz, I., 2019b. Green synthesis of the innovative super paramagnetic nanoparticles from the leaves extract of Fraxinus chinensis Roxb and their application for the decolourisation of toxic dyes. Green Process. Synth. 8, 256–271.

Ali, I., Peng, C., Lin, D., Saroj, D.P., Naz, I., Khan, Z.M., Sultan, M., Ali, M., 2019c. Encapsulated green magnetic nanoparticles for the removal of toxic Pb^{2+} and Cd^{2+} from water: Development, characterization and application. J. Environ. Manage. 234, 273–289.

Ali, I., Peng, C., Naz, I., 2019d. Removal of lead and cadmium ions by single and binary systems using phytogenic magnetic nanoparticles functionalized by 3-marcaptopropanic acid. Chinese J. Chem. Eng. 27, 949–964.

Ali, I., Peng, C., Naz, I., Khan, Z.M., Sultan, M., Islam, T., Abbasi, I.A., 2017. Phytogenic magnetic nanoparticles for wastewater treatment: a review. RSC Adv. 7, 40158–40178.

Alipanahpour Dil, E., Ghaedi, M., Asfaram, A., Mehrabi, F., Bazrafshan, A.A., 2018. Optimization of process parameters for determination of trace Hazardous dyes from industrial wastewaters based on nanostructures materials under ultrasound energy. Ultrason. Sonochem. 40, 238–248.

Alipanahpour Dil, E., Ghaedi, M., Asfaram, A., Mehrabi, F., Bazrafshan, A.A., Tayebi, L., 2019. Synthesis and application of Ce-doped TiO_2 nanoparticles loaded on activated carbon for ultrasound-assisted adsorption of Basic Red 46 dye. Ultrason. Sonochem. 58, 104702.

An, Y., Zheng, H., Sun, Q., Zheng, X., Liu, W., Tang, X., Xiong, Z., 2020a. Two-step synthesis of a single-layer grafting self-floating adsorbent for anionic dyes adsorption, surface separation and concentration. J. Hazard. Mater. 384, 121262.

An, Y., Zheng, H., Sun, Q., Zheng, X., Wu, Q., Zhao, R., 2019a. A novel floating adsorbents system of acid orange 7 removal: Polymer grafting effect. Sep. Purif. Technol. 227, 115677.

An, Y., Zheng, H., Yu, Z., Sun, Y., Wang, Y., Zhao, C., Ding, W., 2020b. Functioned hollow glass microsphere as a self-floating adsorbent: Rapid and high-efficient removal of anionic dye. J. Hazard. Mater. 381, 120971.

An, Y., Zheng, H., Zheng, X., Sun, Q., Zhou, Y., 2019b. Use of a floating adsorbent to remove dyes from water: A novel efficient surface separation method. J. Hazard. Mater. 375, 138–148.

Bhaumik, R., Mondal, N.K., 2016. Optimizing adsorption of fluoride from water by modified banana peel dust using response surface modelling approach. Appl. Water Sci. 6, 115–135.

Blanton, T.N., Huang, T.C., Toraya, H., Hubbard, C.R., Robie, S. B., Louër, D., Göbel, H.E., Will, G., Gilles, R., Raftery, T., 1995. JCPDS—International Centre for Diffraction Data round robin study of silver behenate. A possible low-angle X-ray diffraction calibration standard. Powder Diffr. 10, 91–95.

Chatterjee, A., Abraham, J., 2019. Desorption of heavy metals from metal loaded sorbents and e-wastes: A review. Biotechnol. Lett. 41, 319–333.

Chen, J., Wang, X., Huang, Y., Lv, S., Cao, X., Yun, J., Cao, D., 2018. Adsorption Removal of Pollutant Dyes in Wastewater by Nitrogen-doped Porous Carbons Derived from Natural Leaves. Eng. Sci. https://doi.org/10.30919/es8d666.

Chukwuemeka-Okorie, H.O., Ekemezie, P.N., Akpomie, K.G., Olikagu, C.S., 2018. Calcined corncob-kaolinite Combo as new sorbent for sequestration of toxic metal ions from polluted aqua media and desorption. Front. Chem. 6, 1–13.

Crini, G., Torri, G., Lichtfouse, E., Kyzas, G.Z., Wilson, L.D., Morin-Crini, N., 2019. Dye removal by biosorption using cross-linked chitosan-based hydrogels. Environ. Chem. Lett. 17, 1645–1666.

Dai, Q., Yuan, B., Guo, M., Zhang, K., Chen, X., Song, Z., Nguyen, T.T., Wang, X., Lin, S., Fan, J., Li, Y., Liu, H., Guo, Z., 2020. A novel nano-fibriform C- modified niobium pentoxide by using cellulose templates with highly visible-light photocatalytic performance. Ceram. Int. 46, 13210–13218.

David, M.K., Okoro, U.C., Akpomie, K.G., Okey, C., Oluwasola, H. O., 2020. Thermal and hydrothermal alkaline modification of kaolin for the adsorptive removal of lead(II) ions from aqueous solution. SN Appl. Sci. 2, 1134.

Dawodu, F.A., Akpomie, K.G., 2014. Simultaneous adsorption of Ni (II) and Mn(II) ions from aqueous solution unto a Nigerian kaolinite clay. J. Mater. Res. Technol. 3, 129–141.

Dawodu, M.O., Akpomie, K.G., 2016. Evaluating the potential of a Nigerian soil as an adsorbent for tartrazine dye: Isotherm, kinetic and thermodynamic studies. Alexandria Eng. J. 55, 3211–3218.

Dbik, A., Bentahar, S., El Khomri, M., El Messaoudi, N., Lacherai, A., 2020. Adsorption of Congo red dye from aqueous solutions using tunics of the corm of the saffron. Mater. Today Proc. 22, 134–139.

De Gisi, S., Lofrano, G., Grassi, M., Notarnicola, M., 2016. Characteristics and adsorption capacities of low-cost sorbents for wastewater treatment: A review. Sustain. Mater. Technol. 9, 10–40.

Dehmani, Y., Alrashdi, A.A., Lgaz, H., Lamhasni, T., Abouarnadasse, S., Chung, I.-M., 2020. Removal of phenol from aqueous solution by adsorption onto hematite (α-Fe2O3): Mechanism exploration from both experimental and theoretical studies. Arab. J. Chem. 13(5), 5474–5486. https://doi.org/10.1016/j.arabjc.2020.03.026..

Dhananasekaran, S., Palanivel, R., Pappu, S., 2016. Adsorption of Methylene Blue, Bromophenol Blue, and Coomassie Brilliant Blue by α-chitin nanoparticles. J. Adv. Res. 7, 113–124.

Dil, E.A., Ghaedi, M., Ghezelbash, G.R., Asfaram, A., Ghaedi, A. M., Mehrabi, F., 2016. Modeling and optimization of Hg^{2+} ion biosorption by live yeast Yarrowia lipolytica 70562 from aqueous solutions under artificial neural network-genetic algorithm and response surface methodology: kinetic and equilibrium study. RSC Adv. 6, 54149–54161.

Du, Y., Dai, M., Cao, J., Peng, C., Ali, I., Naz, I., Li, J., 2020. Efficient removal of acid orange 7 using a porous adsorbent-supported zero-valent iron as a synergistic catalyst in advanced oxidation process. Chemosphere 244, 125522.

El-Gamal, S.M.A., Amin, M.S., Ahmed, M.A., 2015. Removal of methyl orange and bromophenol blue dyes from aqueous solution using Sorel's cement nanoparticles. J. Environ. Chem. Eng. 3, 1702–1712.

El-Zahhar, A.A., Awwad, N.S., El-Katori, E.E., 2014. Removal of bromophenol blue dye from industrial waste water by synthesizing polymer-clay composite. J. Mol. Liq. 199, 454–461.

Eze, S.I., Akpomie, K.G., Ezeofor, C.C., Osunkunle, A.A., Maduekwe, O.B., Okenyeka, O.U., 2019. Isotherm and Kinetic Evaluation of Dialium guineense Seed Husk and Its Modified Derivative as Efficient Sorbent for Crude Oil Polluted Water Treatment. Water Conserv. Sci. Eng. 4, 21–31.

Ezekoye, O.M., Akpomie, K.G., Eze, S.I., Chukwujindu, C.N., Ani, J.U., Ujam, O.T., 2020. Biosorptive interaction of alkaline modified Dialium guineense seed powders with ciprofloxacin in contaminated solution: central composite, kinetics, isotherm, thermodynamics, and desorption. Int. J. Phytoremediation, 1–10. https://doi.org/10.1080/15226514.2020.1725869.

Fathy, M., Moghny, T.A., Mousa, M.A., Abdelraheem, O.H., Emam, A.A., 2019. Synthesis and study bromophenol blue dye adsorption efficiency of reduced graphene oxide produced by catalytic acid spray (CAS) method. J. Aust. Ceram. Soc. https://doi.org/10.1007/s41779-019-00367-x.

Feiqiang, G., Xiaolei, L., Xiaochen, J., Xingmin, Z., Chenglong, G., Zhonghao, R., 2018. Characteristics and toxic dye adsorption of magnetic activated carbon prepared from biomass waste by modified one-step synthesis. Colloids Surf. A Physicochem. Eng. Asp. 555, 43–54.

Foo, K.Y., Hameed, B.H., 2010. Insights into the modeling of adsorption isotherm systems. Chem. Eng. J. 156, 2–10.

Fu, Q., Cao, H., Liang, G., Luo, L., Chen, Y., Murugadoss, V., Wu, S., Ding, T., Lin, C., Guo, Z., 2020. A highly Li^+-conductive $HfNb_{24}O_{62}$ anode material for superior Li^+ storage. Chem. Commun. 56, 619–622.

Gautam, R.K., Mudhoo, A., Lofrano, G., Chattopadhyaya, M.C., 2014. Biomass-derived biosorbents for metal ions sequestration: Adsorbent modification and activation methods and adsorbent regeneration. J. Environ. Chem. Eng. 2, 239–259.

Ge, M., Xi, Z., Zhu, C., Liang, G., Hu, G., Jamal, L., S. M., J., 2019. Preparation and Characterization of Magadiite–Magnetite Nanocomposite with Its Sorption Performance Analyses on Removal of Methylene Blue from Aqueous Solutions. Polymers (Basel). 11, 607.

Ghaedi, M., Ghaedi, A.M., Negintaji, E., Ansari, A., Vafaei, A., Rajabi, M., 2014. Random forest model for removal of bromophenol blue using activated carbon obtained from Astragalus bisulcatus tree. J. Ind. Eng. Chem. 20, 1793–1803.

Görgün, N., Özer, Ç., Polat, K., 2019. A new catalyst material from electrospun PVDF-HFP nanofibers by using magnetron-sputter coating for the treatment of dye-polluted waters. Adv. Compos. Hybrid Mater. 2, 423–430.

Haldorai, Y., Kharismadewi, D., Tuma, D., Shim, J.-J., 2015. Properties of chitosan/magnetite nanoparticles composites for

efficient dye adsorption and antibacterial agent. Korean J. Chem. Eng. 32, 1688–1693.
Iqbal, M.J., Ashiq, M.N., 2007. Adsorption of dyes from aqueous solutions on activated charcoal. J. Hazard. Mater. 139, 57–66.
Islam, T., Peng, C., Ali, I., Li, J., Khan, Z.M., Sultan, M., Naz, I., 2020. Synthesis of Rice Husk-Derived Magnetic Biochar Through Liquefaction to Adsorb Anionic and Cationic Dyes from Aqueous Solutions. Arab. J. Sci. Eng. https://doi.org/10.1007/s13369-020-04537-z.
Jabar, J.M., Odusote, Y.A., 2020. Removal of cibacron blue 3G-A (CB) dye from aqueous solution using chemo-physically activated biochar from oil palm empty fruit bunch fiber. Arab. J. Chem. 13 (5), 5417–5429. https://doi.org/10.1016/j.arabjc.2020.03.020.
Jiao, Y., Han, D., Lu, Y., Rong, Y., Fang, L., Liu, Y., Han, R., 2017. Characterization of pine-sawdust pyrolytic char activated by phosphoric acid through microwave irradiation and adsorption property toward CDNB in batch mode. Desalin. Water Treat. 77, 247–255.
Kaur, D., Bagga, V., Behera, N., Thakral, B., Asija, A., Kaur, J., Kaur, S., 2019. SnSe/SnO_2 nanocomposites: novel material for photocatalytic degradation of industrial waste dyes. Adv. Compos. Hybrid Mater. 2, 763–776.
Khoshsang, H., Ghaffarinejad, A., Kazemi, H., Wang, Y., Arandiyan, H., 2018. One-pot synthesis of S-doped Fe_2O_3/C magnetic nanocomposite as an adsorbent for anionic dye removal: equilibrium and kinetic studies. J. Nanostructure Chem. 8, 23–32.
Kocaman, S., 2020. Removal of methylene blue dye from aqueous solutions by adsorption on levulinic acid-modified natural shells. Int. J. Phytoremediation, 1–11. https://doi.org/10.1080/15226514.2020.1736512.
Kyzas, G.Z., Deliyanni, E.A., Lazaridis, N.K., 2014. Magnetic modification of microporous carbon for dye adsorption. J. Colloid Interface Sci. 430, 166–173.
Li, C., Chen, D., Ding, J., Shi, Z., 2020. A novel hetero-exopolysaccharide for the adsorption of methylene blue from aqueous solutions: Isotherm, kinetic, and mechanism studies. J. Clean. Prod. 265, 121800.
Li, N., Zhang, F., Wang, H., Hou, S., 2019. Catalytic Degradation of 4-Nitrophenol in Polluted Water by Three-Dimensional Gold Nanoparticles/Reduced Graphene Oxide Microspheres. Eng. Sci. https://doi.org/10.30919/es8d509.
Liu, J., Yao, S., Wang, L., Zhu, W., Xu, J., Song, H., 2014. Adsorption of bromophenol blue from aqueous samples by novel supported ionic liquids. J. Chem. Technol. Biotechnol. 89, 230–238.
Luo, X.-L., Pei, F., Wang, W., Qian, H., Miao, K.-K., Pan, Z., Chen, Y.-S., Feng, G.-D., 2018. Microwave synthesis of hierarchical porous materials with various structures by controllable desilication and recrystallization. Micropor. Mesopor. Mater. 262, 148–153.
Madrakian, T., Afkhami, A., Mahmood-Kashani, H., Ahmadi, M., 2013. Adsorption of some cationic and anionic dyes on magnetite nanoparticles-modified activated carbon from aqueous solutions: Equilibrium and kinetics study. J. Iran. Chem. Soc. 10, 481–489.
Malana, M.A., Ijaz, S., Ashiq, M.N., 2010. Removal of various dyes from aqueous media onto polymeric gels by adsorption process: Their kinetics and thermodynamics. Desalination 263, 249–257.
Mazaheri, H., Ghaedi, M., Asfaram, A., Hajati, S., 2016. Performance of CuS nanoparticle loaded on activated carbon in the adsorption of methylene blue and bromophenol blue dyes in binary aqueous solutions: Using ultrasound power and optimization by central composite design. J. Mol. Liq. 219, 667–676.
Mehrabi, F., Alipanahpour Dil, E., 2017. Investigate the ultrasound energy assisted adsorption mechanism of nickel(II) ions onto modified magnetic cobalt ferrite nanoparticles: Multivariate optimization. Ultrason. Sonochem. 37, 37–46.
Mohammed, A.A., Al-Musawi, T.J., Kareem, S.L., Zarrabi, M., Al-Ma'abreh, A.M., 2020. Simultaneous adsorption of tetracycline, amoxicillin, and ciprofloxacin by pistachio shell powder coated with zinc oxide nanoparticles. Arab. J. Chem. 13, 4629–4643.
Mohanta, D., Ahmaruzzaman, M., 2018. Bio-inspired adsorption of arsenite and fluoride from aqueous solutions using activated carbon@SnO_2 nanocomposites: Isotherms, kinetics, thermodynamics, cost estimation and regeneration studies. J. Environ. Chem. Eng. 6, 356–366.
Momina, M., Shahadat, M., Isamil, S., 2018. Regeneration performance of clay-based adsorbents for the removal of industrial dyes: a review. RSC Adv. 8, 24571–24587.
Mtshatsheni, K.N.G., Ofomaja, A.E., Naidoo, E.B., 2019. Synthesis and optimization of reaction variables in the preparation of pine-magnetite composite for removal of methylene blue dye. South African J. Chem. Eng. 29, 33–41.
Muhammad, A., Shah, A.-H.A., Bilal, S., Rahman, G., 2019. Basic Blue Dye Adsorption from Water Using Polyaniline/Magnetite (Fe_3O_4) Composites: Kinetic and Thermodynamic Aspects. Materials (Basel). 12, 1764.
Nassar, M.Y., Ahmed, I.S., Hendy, H.S., 2018. A facile one-pot hydrothermal synthesis of hematite (α-Fe_2O_3) nanostructures and cephalexin antibiotic sorptive removal from polluted aqueous media. J. Mol. Liq. 271, 844–856.
Nassar, M.Y., Ahmed, I.S., Raya, M.A., 2019. A facile and tunable approach for synthesis of pure silica nanostructures from rice husk for the removal of ciprofloxacin drug from polluted aqueous solutions. J. Mol. Liq. 282, 251–263.
Nassar, M.Y., Ali, E.I., Zakaria, E.S., 2017. Tunable auto-combustion preparation of TiO_2 nanostructures as efficient adsorbents for the removal of an anionic textile dye. RSC Adv. 7, 8034–8050.
Nessim, R.B., Bassiouny, A.R., Zaki, H.R., Moawad, M.N., Kandeel, K.M., 2011. Biosorption of lead and cadmium using marine algae. Chem. Ecol. 27, 579–594.
Nsom, M.V., Etape, E.P., Tendo, J.F., Namond, B.V., Chongwain, P.T., Yufanyi, M.D., William, N., 2019. A Green and Facile Approach for Synthesis of Starch-Pectin Magnetite Nanoparticles and Application by Removal of Methylene Blue from Textile Effluent. J. Nanomater. 2019, 1–12.
Ogbu, I., Akpomie, K., Osunkunle, A., Eze, S., 2019. Sawdust-kaolinite composite as efficient sorbent for heavy metal ions. Bangladesh J. Sci. Ind. Res. 54, 99–110.
Olu-Owolabi, B.I., Diagboya, P.N., Ebaddan, W.C., 2012. Mechanism of Pb^{2+} removal from aqueous solution using a nonliving moss biomass. Chem. Eng. J. 195–196, 270–275.
Oyekanmi, A.A., Ahmad, A., Hossain, K., Rafatullah, M., 2019. Adsorption of Rhodamine B dye from aqueous solution onto acid treated banana peel: Response surface methodology, kinetics and isotherm studies. PLoS One 14, e0216878.
Rai, M.K., Shahi, G., Meena, V., Meena, R., Chakraborty, S., Singh, R.S., Rai, B.N., 2016. Removal of hexavalent chromium Cr(VI) using activated carbon prepared from mango kernel activated with H_3PO_4. Resour. Technol. 2, S63–S70.
Rajapaksha, A.U., Chen, S.S., Tsang, D.C.W., Zhang, M., Vithanage, M., Mandal, S., Gao, B., Bolan, N.S., Ok, Y.S., 2016. Engineered/designer biochar for contaminant removal/immobilization from soil and water: Potential and implication of biochar modification. Chemosphere 148, 276–291.
Rajput, S., Pittman, C.U., Mohan, D., 2016. Magnetic magnetite (Fe_3O_4) nanoparticle synthesis and applications for lead (Pb^{2+}) and chromium (Cr^{6+}) removal from water. J. Colloid Interface Sci. 468, 334–346.
Şenol, Z.M., 2020. Effective biosorption of Allura red dye from aqueous solutions by the dried-lichen (Pseudoevernia furfuracea) biomass. Int. J. Environ. Anal. Chem., 1–15
Shakoor, S., Nasar, A., 2016. Removal of methylene blue dye from artificially contaminated water using citrus limetta peel waste as a very low cost adsorbent. J. Taiwan Inst. Chem. Eng. 66, 154–163.
Shang, Y., Cui, Y., Shi, R., Yang, P., Wang, J., Wang, Y., 2019. Regenerated WO2.72 nanowires with superb fast and selective

adsorption for cationic dye: Kinetics, isotherm, thermodynamics, mechanism. J. Hazard. Mater. 379, 120834.

Shi, C., Qi, H., Sun, Z., Qu, K., Huang, Z., Li, J., Dong, M., Guo, Z., 2020a. Carbon dot-sensitized urchin-like Ti^{3+} self-doped TiO_2 photocatalysts with enhanced photoredox ability for highly efficient removal of Cr^{6+} and RhB. J. Mater. Chem. C 8, 2238–2247. https://doi.org/10.1039/C9TC05513D.

Shi, X., Wang, C., Ma, Y., Liu, H., Wu, S., Shao, Q., He, Z., Guo, L., Ding, T., Guo, Z., 2019. Template-free microwave-assisted synthesis of FeTi coordination complex yolk-shell microspheres for superior catalytic removal of arsenic and chemical degradation of methylene blue from polluted water. Powder Technol. 356, 726–734.

Shi, X., Wang, C., Zhang, J., Guo, L., Lin, J., Pan, D., Zhou, J., Fan, J., Ding, T., Guo, Z., 2020b. Zwitterionic glycine modified Fe/Mg-layered double hydroxides for highly selective and efficient removal of oxyanions from polluted water. J. Mater. Sci. Technol. 51, 8–15.

Singh, N., Jana, S., Singh, G.P., Dey, R.K., 2020a. Graphene-supported TiO_2: study of promotion of charge carrier in photocatalytic water splitting and methylene blue dye degradation. Adv. Compos. Hybrid Mater. 3, 127–140.

Singh, S., Kumar, V., Datta, S., Dhanjal, D.S., Sharma, K., Samuel, J., Singh, J., 2020b. Current advancement and future prospect of biosorbents for bioremediation. Sci. Total Environ. 709. https://doi.org/10.1016/j.scitotenv.2019.135895.

Song, B., Wang, Q., Wang, L., Lin, J., Wei, X., Murugadoss, V., Wu, S., Guo, Z., Ding, T., Wei, S., 2020. Carbon nitride nanoplatelet photocatalysts heterostructured with B-doped carbon nanodots for enhanced photodegradation of organic pollutants. J. Colloid Interface Sci. 559, 124–133.

Song, J., Wang, Y., Qiu, J., 2018. High Adsorption Performance of Methyl Blue from Aqueous Solution Using Hyperbranched Polyethyleneimine Grafted MWCNTs as an Adsorbent. ES Mater. Manuf. https://doi.org/10.30919/esmm5f193.

Stavrinou, A., Aggelopoulos, C.A., Tsakiroglou, C.D., 2018. Exploring the adsorption mechanisms of cationic and anionic dyes onto agricultural waste peels of banana, cucumber and potato: Adsorption kinetics and equilibrium isotherms as a tool. J. Environ. Chem. Eng. 6, 6958–6970.

Sun, K., Wang, L., Wang, Zongxiang, Wu, X., Fan, G., Wang, Zhongyang, Cheng, C., Fan, R., Dong, M., Guo, Z., 2020. Flexible silver nanowire/carbon fiber felt metacomposites with weakly negative permittivity behavior. Phys. Chem. Chem. Phys. 22, 5114–5122.

Trinh, V.T., Minh, T., Nguyen, P., Van, H.T., Hoang, L.P., 2020. Phosphate Adsorption by Silver Nanoparticles-Loaded Activated Carbon derived from Tea Residue. Sci. Rep. 10, 3634.

Wang, Z., Sun, K., Xie, P., Hou, Q., Liu, Y., Gu, Q., Fan, R., 2020. Design and analysis of negative permittivity behaviors in barium titanate/nickel metacomposites. Acta Mater. 185, 412–419.

Xia, X., Xu, X., Lin, C., Yang, Y., Zeng, L., Zheng, Y., Wu, X., Li, W., Xiao, L., Qian, Q., Chen, Q., 2020. Microalgal-Immobilized Biocomposite Scaffold Fabricated by Fused Deposition Modeling 3D Printing Technology for Dyes Removal. ES Mater. Manuf. https://doi.org/10.30919/esmm5f706.

Xiang, Y., Gao, M., Shen, T., Cao, G., Zhao, B., Guo, S., 2019. Comparative study of three novel organo-clays modified with imidazolium-based gemini surfactant on adsorption for bromophenol blue. J. Mol. Liq. 286, 110928.

Yadav, S., Asthana, A., Chakraborty, R., Jain, B., Singh, A.K., Carabineiro, S.A.C., Susan, M.A.B.H., 2020. Cationic Dye Removal Using Novel Magnetic/Activated Charcoal/β-Cyclodextrin/Alginate Polymer Nanocomposite. Nanomaterials 10, 170.

You, L., Wu, Z., Kim, T., Lee, K., 2006. Kinetics and thermodynamics of bromophenol blue adsorption by a mesoporous hybrid gel derived from tetraethoxysilane and bis(trimethoxysilyl)hexane. J. Colloid Interface Sci. 300, 526–535.

You, Y., KeqiQu, Huang, Z., Ma, R., Shi, C., Li, X., Liu, D., Dong, M., Guo, Z., 2019. Sodium alginate templated hydroxyapatite/calcium silicate composite adsorbents for efficient dye removal from polluted water. Int. J. Biol. Macromol. 141, 1035–1043.

Zhang, Y., Shao, Q., Chen, C., Jiang, H., Su, F., Hu, Q., Guo, Z., 2020. Microwave-hydrothermal synthesis of beta-bismuth(III)oxide nanopowders and their enhanced photocatalytic properties. Powder Technol. 370, 226–236.

Zhao, W., Li, X., Yin, R., Qian, L., Huang, X., Liu, H., Zhang, J., Wang, J., Ding, T., Guo, Z., 2019. Urchin-like NiO–$NiCo_2O_4$ heterostructure microsphere catalysts for enhanced rechargeable non-aqueous Li–O_2 batteries. Nanoscale 11, 50–59.